



Jeng-Tzong Chen · Jeng-Hong Kao · Yi-Ling Huang ·  
Shing-Kai Kao

# On the stress concentration factor of circular/elliptic hole and rigid inclusion under the remote anti-plane shear by using degenerate kernels

Received: 1 May 2020 / Accepted: 9 October 2020 / Published online: 10 February 2021  
© Springer-Verlag GmbH Germany, part of Springer Nature 2021

**Abstract** The stress concentration factor (SCF) along the boundary of a hole and a rigid inclusion in an infinite isotropic solid under the anti-plane shear is revisited by using degenerate kernels in the boundary integral equation (BIE) although this result was obtained by invoking the extended circle theorem of Milne-Thomson as well as the complex variable approach. The degenerate kernel of series form for the closed-form fundamental solution is used for the circle and the ellipse in terms of polar and elliptic coordinates, respectively. The slender ratio of the ellipse and the orientation are two parameters for our study. The strain energy density along the boundary is increased or decreased due to the different types of loading and various aspect ratios of the ellipse. An analytical solution for the SCF is then derived for any orientation of the ellipse relative to the applied load. The reciprocal relation for the SCF between a hole and a rigid inclusion with respect to different loading is also addressed. Besides, this analytical derivation can clearly show the appearing mechanism why the BEM/BIEM suffers the degenerate scale in the rigid inclusion.

**Keywords** Stress concentration factor · Anti-plane shear · Degenerate kernel · Rigid inclusion

## 1 Introduction

The problem of SCF around holes or rigid inclusions under the remote anti-plane shear loading has been investigated by many researchers, but mostly analytical solutions have been derived primarily for an infinite plane by using the complex variables of analytical functions. A comparison of the stress concentration around the circular holes between the theory [1] and experiments was studied by Meguid and Gong [2]. An experimental proof of stress concentrations around stiff rectangular and rhombohedral inclusions has been provided by using

---

J.-T. Chen (✉) · J.-H. Kao · Y.-L. Huang · S.-K. Kao  
Department of Harbor and River Engineering, National Taiwan Ocean University, Keelung 20224, Taiwan  
E-mail: jtchen@mail.ntou.edu.tw

J.-T. Chen  
Department of Mechanical and Mechatronic Engineering, National Taiwan Ocean University, Keelung 20224, Taiwan

J.-T. Chen  
Department of Civil Engineering, National Cheng Kung University, Tainan 70101, Taiwan

J.-T. Chen  
Bachelor Degree Program in Ocean Engineering and Technology, National Taiwan Ocean University, Keelung 20224, Taiwan

J.-T. Chen  
Center of Excellence for Ocean Engineering, National Taiwan Ocean University, Keelung 20224, Taiwan

photoelasticity [3]. Furthermore, real engineering experiments on mortar specimens containing inclusions have been conducted [4].

Here, we focus on our attention to the problem of anti-plane elasticity which is sometimes considered due to not only its mathematical abstraction but also its popularity for the anti-plane shear problem of holes or inclusions embedded in an infinite elastic plane containing in fiber-reinforced composites and crack. Chen et al. [5] evaluated the degenerate scale for BIE in plane elasticity and anti-plane elasticity by using conformal mapping. Zou [6] investigated Eshelby's anti-plane inclusion problem of a cylindrical isotropic elastic body with finite but arbitrary cross section. Some real examples of anti-plane problems were reported. Most often, the anti-plane problem of an inclusion has been investigated with respect to uniform boundary conditions [7–9]. The nonuniform loading has also been studied [10–12]. Savin [13] gave a wide variety of hole shapes and a number of different multiple-hole patterns under different loading conditions.

Recently, Lubarda [14] revisited the analytical solution of anti-plane shear problems for the circumferential shear stress around circular and elliptic holes, the strain energy and SCFs were also discussed. Noda and Takase [15] considered stress concentration formulas for all notch shape by using the body force method. He gave an example of anti-plane shear to explain the fundamental ideas. Honein et al. [16] have solved problems of two arbitrary circular holes or rigid inclusions of different shear moduli under the remote shear. They have introduced the Möbius transformation involving the complex potential to analytically investigate the stress field around the hole. Since the extension to more than two holes may have difficulty in the Möbius formulation, NTOU/MSV group [17] proposed a semi-analytical approach, so-called the null-field integral formulation to solve problems containing several circular holes. The key idea is that they employed the degenerate kernel to solve the BIE in conjunction with the adaptive observer system. Although the degenerate kernel plays an important role in the theory of integral equations and gives a natural approximation, its use in engineering problems seems to have taken a back seat to other methods such as quadrature and collocation as quoted by Golberg [18]. In the literature, only few researchers have applied the degenerate kernel to solve boundary value problems. Golberg [18] pointed out the potential power of degenerate kernel in the BIE as well as BEM, while Galybin [19] solved the crack problems by using the degenerate kernel. Mathematically speaking, the integral equation is nothing more than the linear algebra [20], once the degenerate kernel is available. In this regard, we will demonstrate how the analytical tool, degenerate kernel, can solve the anti-plane shear problems containing a circular and an elliptic hole or rigid inclusion. Lee and Chen [21] first proposed the degenerate kernel in terms of elliptic coordinates and combined the null-field integral approach to deal with the anti-plane problem. However, they did not focus on the SCF of the single elliptic/circular hole and rigid inclusions. For the 3-D rigid inclusion problem, the interaction between elliptic and ellipsoidal inclusion under bending stress fields were also addressed by Noda and Hayashida [22].

Despite the fact that nowadays FEM, BEM and meshless methods can numerically solve the problem, a closed-form solution is still eagerly preferred over the numerical results mainly for two reasons. First, an analytical solution can be chosen as a benchmark example for verifying the accuracy of numerical results. Secondly, and more definitely, the solution space of an analytical solution often leads to the clear understanding of influence of parameter on the solution and get more physical insights into the problem under consideration which may sometimes yield surprising and counter-intuitive features of the general solution. This is the reason why we revisit the analytical solution by using the degenerate kernel instead of the complex variables. To extend to the three dimensional case, our approach is more promising while the complex variables may be hindered.

The stress field of infinite domain with a circular hole under the remote anti-plane shear follows from a version of the Milne-Thomson circle theorem [23] for the two-dimensional irrotational flow of an incompressible inviscid fluid. Complex variables in companion with the analytical function is now a classical tool to solve such a problem. Here, we will employ the degenerate kernel in the BIE to revisit this problem. Not only a circular/elliptic hole but also circular/elliptic rigid inclusion will be demonstrated by using the degenerate kernels in terms of polar and elliptical coordinates, respectively. Parameter study of the slender ratio and the orientation angle of the ellipse will be done. The occurring mechanism of the degenerate scale in the BEM/BIEM will also be examined only for the case of rigid inclusion instead of hole. The paper is organized as follows: Sects. 2.1 and 2.2 begin with analytical solutions for the displacement of an infinite elastic body containing a circular hole and an elliptic hole under the remote anti-plane shear by using the degenerate kernel, respectively. Sections 3.1 and 3.2 present analytical solutions for the displacement of an infinite elastic body containing a circular rigid inclusion and an elliptic rigid inclusion under the remote anti-plane shear by using the degenerate kernel, respectively. Section 4 present the SCF value of the examples in Sects. 2–3, the general formula and present approach we used will be compared. The reciprocal relation for the SCF between a hole

and a rigid inclusion with respect to different loading is also addressed. Section 5 presents the strain energy, and all figures match well with those of Lubarda [14] although a different approach using the degenerate kernel is employed. Section 6 concludes with remarks about related and future work.

**2 Analytical solution of an infinite elastic body containing circular hole or an elliptic hole under the remote anti-plane shear by using the degenerate kernel**

2.1 A circular hole under the remote anti-plane shear ( $\sigma_{yz}^\infty = S$  and  $\sigma_{xz}^\infty = 0$ ) and ( $\sigma_{yz}^\infty = 0$  and  $\sigma_{xz}^\infty = S$ )

The displacements for the anti-plane shear problem are given by

$$(u_x, u_y, u_z) = (0, 0, u_z(x, y)), \tag{1}$$

where  $u_z$  is the only nonvanishing component of displacement with respect to the Cartesian coordinates which is a function of  $x$  and  $y$  only. Thus, the nonvanishing shear strains are given by

$$\varepsilon_{xz} = \frac{1}{2} \frac{\partial u_z}{\partial x}, \quad \varepsilon_{yz} = \frac{1}{2} \frac{\partial u_z}{\partial y}, \tag{2}$$

and the corresponding stresses follow Hooke’s law

$$\sigma_{xz} = 2\mu\varepsilon_{xz}, \quad \sigma_{yz} = 2\mu\varepsilon_{yz}, \tag{3}$$

where  $\mu$  is the shear modulus. Therefore, the equilibrium equation reduces to

$$\frac{\partial \sigma_{xz}}{\partial x} + \frac{\partial \sigma_{yz}}{\partial y} = 0, \tag{4}$$

which can be rewritten in terms of the displacement  $u_z$  by using Eqs. (2) and (3) as follows

$$\frac{\partial^2 u_z}{\partial x^2} + \frac{\partial^2 u_z}{\partial y^2} = \nabla^2 u_z = 0. \tag{5}$$

Now, we consider a circular hole in an infinite elastic body under the remote anti-plane shear stress ( $\sigma_{yz}^\infty = S$  and  $\sigma_{xz}^\infty = 0$ ) as shown in Fig. 1, where  $B$  is the boundary and  $a$  is the radius of the circle. The boundary condition on the circular hole is free of traction, which yields the Neumann boundary condition,

$$t(x) = \frac{\partial u_z}{\partial n} = 0, \quad x \in B, \tag{6}$$

where  $n$  is the unit outward normal vector. The shear stress and the displacement at infinity are

$$\sigma_{yz}^\infty = S, \quad |y| \rightarrow \infty, \quad \text{and} \quad u_z^\infty = \frac{Sy}{\mu}, \quad |y| \rightarrow \infty, \tag{7}$$

respectively. By employing the superposition technique, the total displacement is decomposed into two parts as shown in Fig. 1.

One is due to the remote shear loading  $\sigma_{yz}^\infty$  in an infinite plane, and the other  $u_z^M$  is caused by the infinite plane problem with a circular hole. The total displacement can be given as

$$u_z = u_z^\infty + u_z^M. \tag{8}$$

Based on the potential theory, the closed-form fundamental solution in the BEM/BIEM for the Laplace problem is  $U(s, x) = \ln|x - s| = \ln r$ , where  $r$  is the distance between  $x$  and  $s$ . By employing the separable property of the kernel,  $U(s, x)$  can be expanded into the degenerate form by separating the source point and field point in the polar coordinates [24] as given below:

$$U(s, x) = \begin{cases} U^i(R, \theta; \rho, \phi) = \ln R - \sum_{m=1}^{\infty} \frac{1}{m} \left(\frac{\rho}{R}\right)^m \cos m(\theta - \phi), & R \geq \rho, & (a) \\ U^e(R, \theta; \rho, \phi) = \ln \rho - \sum_{m=1}^{\infty} \frac{1}{m} \left(\frac{R}{\rho}\right)^m \cos m(\theta - \phi), & \rho > R, & (b) \end{cases} \tag{9}$$

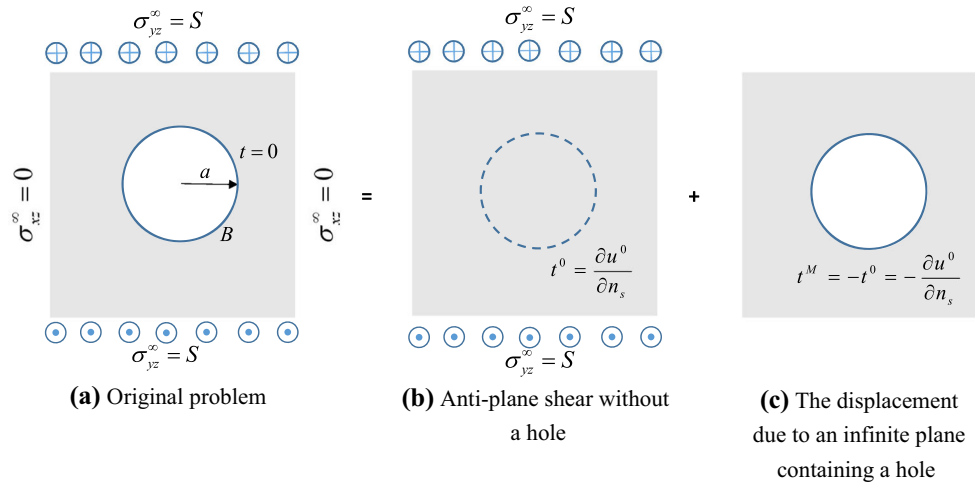


**Fig. 1** A circular hole in an infinite elastic body under the remote anti-plane shear loading ( $\sigma_{yz}^\infty = S$  and  $\sigma_{xz}^\infty = 0$ )

where the field point  $x = (\rho, \phi)$ , the source point  $s = (R, \theta)$ , the superscripts “*i*” and “*e*” denote the interior ( $R > \rho$ ) and exterior ( $\rho > R$ ) cases, respectively. The degenerate-kernel expression for the closed-form fundamental solution is plotted in Fig. 2 to show its radial symmetry of the source behavior. After taking the normal derivative  $-\partial/\partial R$  with respect to the source point,  $T(s, x)$  can be obtained as shown below:

$$T(s, x) = \begin{cases} T^i(R, \theta; \rho, \phi) = -(\frac{1}{R} + \sum_{m=1}^{\infty} (\frac{\rho^m}{R^{m+1}}) \cos m(\theta - \phi)), & R > \rho, & (a) \\ T^e(R, \theta; \rho, \phi) = \sum_{m=1}^{\infty} (\frac{R^{m-1}}{\rho^m}) \cos m(\theta - \phi), & \rho > R. & (b) \end{cases} \quad (10)$$

The integral formulation for the domain point of Laplace problem can be derived from Green’s third identity. By employing the degenerate kernel, the collocation point can be located on the real boundary free of facing the singular integral. Therefore, the representations of conventional integral equations including the boundary point can be written as

$$2\pi u(x) = \int_B T^e(s, x)u(s)dB(s) - \int_B U^e(s, x)t(s)dB(s), \quad x \in D \cup B. \quad (11)$$

The null-field integral equation is represented as

$$0 = \int_B T^i(s, x)u(s)dB(s) - \int_B U^i(s, x)t(s)dB(s), \quad x \in D^c \cup B, \quad (12)$$

where  $D$  is the domain,  $D^c$  is the complementary domain and  $t(s) = \frac{\partial u(s)}{\partial n_s}$ .

Equations (11) and (12) can include the boundary point since a proper degenerate kernel is chosen.

To obtain the total displacement  $u_z$ , we need to solve the unknown displacement  $u_z^M(x)$  first. Since  $u_z^\infty$  is given in Eq. (7), the displacement along the circular boundary in the infinite plane without a hole is

$$u_z^0(s) = \frac{S}{\mu} R \sin \theta, \quad s = (R, \theta) \in B, \quad (13)$$

in polar coordinates. Therefore, we can easily obtain its normal derivative  $t^0$  and  $t^M$  on the boundary

$$t^0(s) = \frac{\partial u_z^0(s)}{\partial n_s} = -\frac{\partial u_z^0(s)}{\partial R} = -\frac{S}{\mu} \sin \theta, \quad s = (R, \theta) \in B, \quad (14)$$

$$t^M(s) = -t^0 = \frac{S}{\mu} \sin \theta, \quad s = (R, \theta) \in B, \quad (15)$$

respectively.

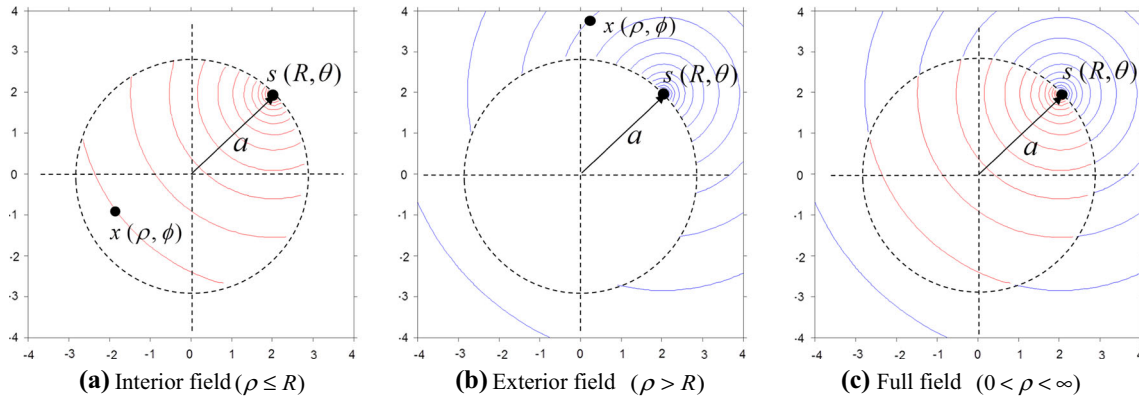


**Fig. 2** Contour plot of the degenerate kernel for the fundamental solution ( $U(s, x)$ ) in polar coordinates,  $R = a$

By applying the Fourier expansions, the specified boundary data  $u_z^M(s)$  along the circular boundary can be expressed by

$$u_z^M(s) = p_0 + \sum_{n=1}^{\infty} p_n \cos n\theta + \sum_{n=1}^{\infty} q_n \sin n\theta, \quad 0 \leq \theta < 2\pi, \quad s = (R, \theta) \in B, \quad (16)$$

where  $p_0, p_n$  and  $q_n$  are the unknown coefficients of Fourier series to be determined. By substituting Eqs. (9a), (10a), (15) and (16) into Eq. (12) for  $dB(s) = a d\theta (R = a)$  and locating  $x$  on the real boundary ( $\rho = a$ ) for the circular hole, we have

$$-2\pi p_0 - \sum_{n=1}^{\infty} \pi \cos(n\phi) p_n - \sum_{n=1}^{\infty} \pi \sin(n\phi) q_n = -\frac{S}{\mu} a \pi \sin(\phi), \quad x = (\rho, \phi) \in B, \quad (17)$$

where  $x$  can be in the domain or on the boundary since a proper degenerate kernel is already chosen. After comparing coefficients of the basis,  $1, \cos n\phi$  and  $\sin n\phi$ , we have

$$\begin{cases} p_n = 0, & n = 0, 1, 2, 3, \dots, \\ q_1 = \frac{S}{\mu} a, & n = 1, \\ q_n = 0, & n = 2, 3, \dots \end{cases} \quad (18)$$

Therefore, Eq. (16) can be written as

$$u_z^M(s) = \frac{S}{\mu} a \sin \theta, \quad s = (R, \theta) \in B. \quad (19)$$

By substituting Eqs. (9b), (10b), (15) and (19) into Eq. (11) for  $dB(s) = a d\theta$ , integration along the real boundary ( $R = a$ ) of the circular hole yields

$$u_z^M(\rho, \phi) = \frac{S}{\mu} \frac{a^2}{\rho} \sin \phi, \quad x = (\rho, \phi) \in D. \quad (20)$$

By substituting Eqs. (7) and (2) into Eq. (8), we have

$$u_z(\rho, \phi) = \frac{S}{\mu} \rho \left( 1 + \frac{a^2}{\rho^2} \right) \sin \phi. \quad (21)$$

The total displacement expressed in the polar coordinates can be obtained in Eq. (21). For the circular hole in the different direction ( $\sigma_{yz}^\infty = 0$  and  $\sigma_{xz}^\infty = S$ ) as shown in Fig. 3. The total displacement can be obtained by replacing  $\phi$  to  $\phi + \pi/2$  in Eq. (21) as

$$u_z(\rho, \phi) = \frac{S}{\mu} \rho \left( 1 + \frac{a^2}{\rho^2} \right) \cos \phi. \quad (22)$$

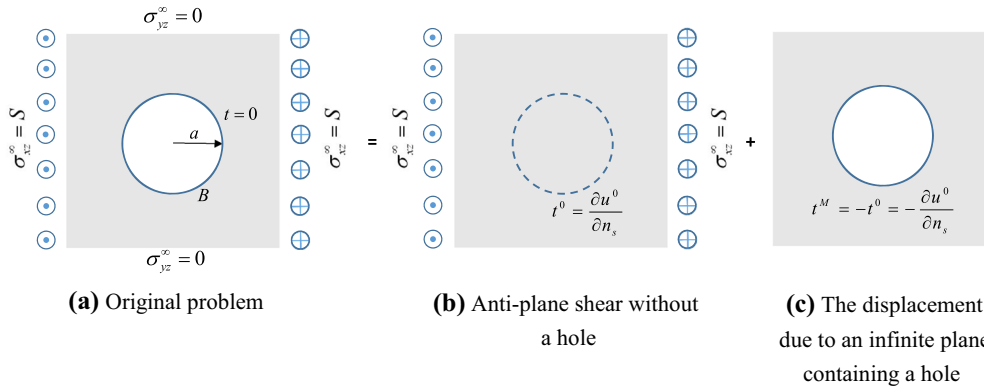


**Fig. 3** A circular hole in an infinite elastic body under the remote anti-plane shear loading ( $\sigma_{yz}^\infty = 0$  and  $\sigma_{xz}^\infty = S$ )

2.2 An elliptic hole under the remote anti-plane shear ( $\sigma_{yz}^\infty = S$  and  $\sigma_{xz}^\infty = 0$ ) and ( $\sigma_{yz}^\infty = 0$  and  $\sigma_{xz}^\infty = S$ )

Now, we consider an elliptic hole in an infinite elastic body under the remote anti-plane shear stress ( $\sigma_{yz}^\infty = S$  and  $\sigma_{xz}^\infty = 0$ ) as shown in Fig. 4,  $B$  is the elliptical boundary of  $\xi = \xi_0 = const.$ ,  $a$  is the semi-major axis and  $b$  is the semi-minor axis of the ellipse. In this case, we follow the similar procedure as the previous section of the circular case. Based on the separable property,  $U(s, x)$  can be expanded into the degenerate form by separating the source point and field point in the elliptic coordinates [25] as given below:

$$U(s, x) = \begin{cases} U^i(\xi_s, \eta_s; \xi_x, \eta_x) = \xi_s + \ln \frac{c}{2} - \sum_{m=1}^{\infty} \frac{2}{m} e^{-m\xi_s} \cosh m\xi_x \cos m\eta_x \cos m\eta_s \\ \quad - \sum_{m=1}^{\infty} \frac{2}{m} e^{-m\xi_s} \sinh m\xi_x \sin m\eta_x \sin m\eta_s, & \xi_s \geq \xi_x, & (a) \\ U^e(\xi_s, \eta_s; \xi_x, \eta_x) = \xi_x + \ln \frac{c}{2} - \sum_{m=1}^{\infty} \frac{2}{m} e^{-m\xi_x} \cosh m\xi_s \cos m\eta_x \cos m\eta_s \\ \quad - \sum_{m=1}^{\infty} \frac{2}{m} e^{-m\xi_x} \sinh m\xi_s \sin m\eta_x \sin m\eta_s, & \xi_s < \xi_x, & (b) \end{cases} \quad (23)$$

where the field point  $x = (\xi_x, \eta_x)$ , the source point  $s = (\xi_s, \eta_s)$ , and  $c$  is the half distance between two foci, the superscripts “ $i$ ” and “ $e$ ” denote the interior ( $\xi_s \geq \xi_x$ ) and exterior ( $\xi_s < \xi_x$ ) cases, respectively. The degenerate-kernel expression for the closed-form fundamental solution is plotted in Fig. 5. After taking the normal derivative with respect to the source point,  $T(s, x)$  can be obtained as shown below:

$$T(s, x) = \begin{cases} T^i(\xi_s, \eta_s; \xi_x, \eta_x) = \frac{-1}{J(\xi_s, \eta_s)} \left( 1 + 2 \sum_{m=1}^{\infty} e^{-m\xi_s} \cosh m\xi_x \cos m\eta_x \cos m\eta_s \right. \\ \quad \left. + 2 \sum_{m=1}^{\infty} e^{-m\xi_s} \sinh m\xi_x \sin m\eta_x \sin m\eta_s \right), & \xi_s > \xi_x, & (a) \\ T^e(\xi_s, \eta_s; \xi_x, \eta_x) = \frac{1}{J(\xi_s, \eta_s)} \left( 2 \sum_{m=1}^{\infty} e^{-m\xi_x} \sinh m\xi_s \cos m\eta_x \cos m\eta_s \right. \\ \quad \left. + 2 \sum_{m=1}^{\infty} e^{-m\xi_x} \cosh m\xi_s \sin m\eta_x \sin m\eta_s \right), & \xi_s < \xi_x. & (b) \end{cases} \quad (24)$$

It is noted that a Jacobian term,  $J(\xi_s, \eta_s) = J_s = c\sqrt{\cosh^2 \xi_s \sin^2 \eta_s + \sinh^2 \xi_s \cos^2 \eta_s}$ , is in the denominator.

Since  $u_z^\infty$  is given in Eq. (7), the displacement along the elliptic boundary in the infinite plane without a hole is

$$u_z^0(s) = \frac{S}{\mu} c \sinh \xi_s \sin \eta_s, \quad s = (\xi_s, \eta_s) \in B, \quad (25)$$

in elliptic coordinates. We can easily obtain its normal derivative  $t^0$  and  $t^M$  on the boundary

$$t^0(s) = \frac{\partial u_z^0(s)}{\partial n_s} = -\frac{1}{J_s} \frac{\partial u_z^0(s)}{\partial \xi_s} = -\frac{S}{J_s \mu} c \cosh \xi_s \sin \eta_s, \quad s = (\xi_s, \eta_s) \in B, \quad (26)$$

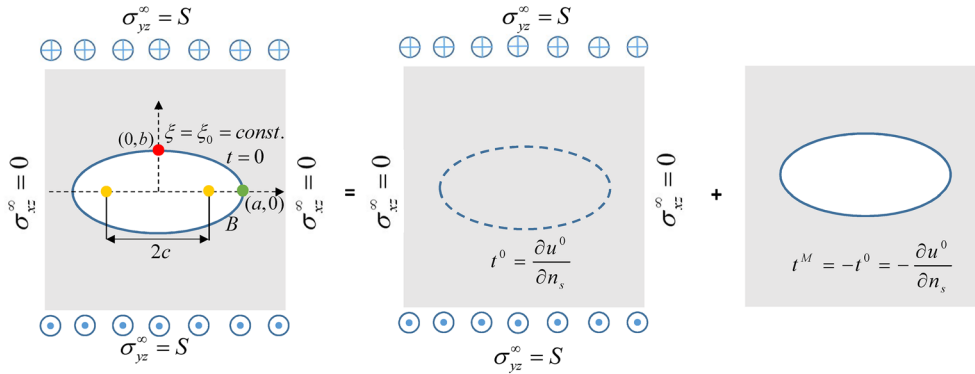


**Fig. 4** An elliptic hole in an infinite elastic body under the remote anti-plane shear loading ( $\sigma_{yz}^\infty = S$  and  $\sigma_{xz}^\infty = 0$ )

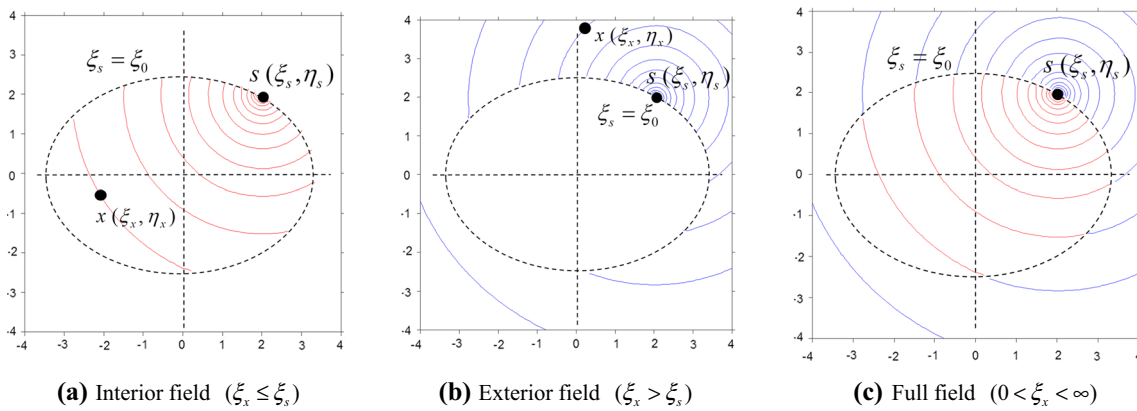


**Fig. 5** Contour plot of the degenerate kernel for the fundamental solution ( $U(s, x)$ ) in elliptic coordinates,  $\xi_s = \xi_0$

$$t^M(s) = -t^0 = \frac{S}{J_s \mu} c \cosh \xi_s \sin \eta_s, \quad s = (\xi_s, \eta_s) \in B, \tag{27}$$

respectively. By applying the Fourier expansions, the specified boundary data  $u_z^M(s)$  along the elliptic boundary ( $\xi_s = \xi_0$  is a constant) can be expressed by

$$u_z^M(s) = p_0 + \sum_{n=1}^{\infty} p_n \cos n\eta_s + \sum_{n=1}^{\infty} q_n \sin n\eta_s, \quad 0 \leq \eta_s < 2\pi, \quad s = (\xi_s, \eta_s) \in B, \tag{28}$$

where  $p_0$ ,  $p_n$  and  $q_n$  are the unknown coefficients of Fourier series to be determined. By substituting Eqs. (23a), (24a), (27) and (28) into Eq. (12), for  $dB(s) = J(\xi_s, \eta_s)d\eta_s$  ( $\xi_s = \xi_0$ ) and locating  $x$  on the real boundary ( $\xi_x = \xi_0$ ) for the elliptic hole, we have

$$\begin{aligned} & -2\pi p_0 - \sum_{n=1}^{\infty} 2\pi e^{-n\xi_0} \cosh n\xi_0 \cos n\eta_x p_n - \sum_{n=1}^{\infty} 2\pi e^{-n\xi_0} \sinh n\xi_0 \sin n\eta_x q_n \\ & = -2\pi \frac{S}{\mu} c e^{-\xi_0} \sinh \xi_0 \cosh \xi_0 \sin \eta_x, \quad x = (\xi_x, \eta_x) \in B, \end{aligned} \tag{29}$$

where  $x$  can be in the domain or on the boundary since a proper degenerate kernel is already chosen. After comparing coefficients of the basis,  $1$ ,  $\cos n\eta_x$  and  $\sin n\eta_x$ , we have

$$\begin{cases} p_n = 0, & n = 0, 1, 2, \dots, \\ q_1 = \frac{S}{\mu} c \sinh \xi_0, & n = 1, \\ q_n = 0, & n = 2, 3, \dots. \end{cases} \tag{30}$$

Therefore, Eq. (28) can be written as

$$u_z^M(s) = \frac{S}{\mu} c \cosh \xi_0 \sin \eta_s, \quad s = (\xi_s, \eta_s) \in B. \tag{31}$$

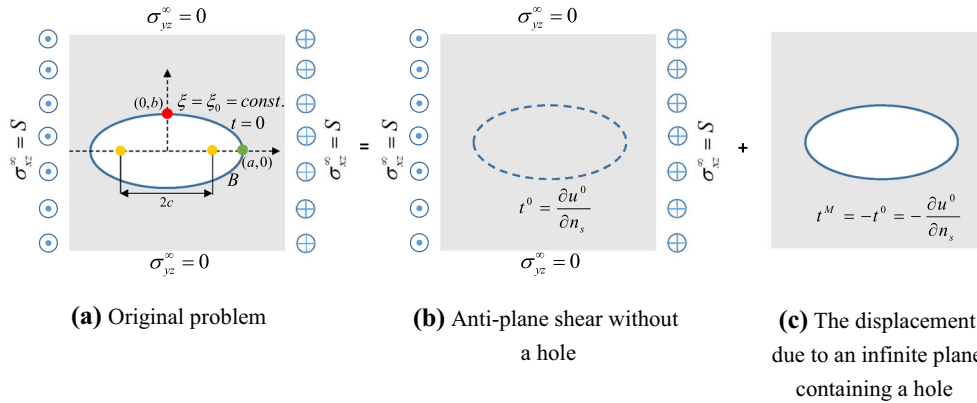


**Fig. 6** An elliptic hole in an infinite elastic body under the remote anti-plane shear loading ( $\sigma_{yz}^\infty = 0$  and  $\sigma_{xz}^\infty = S$ )

By combining Eqs. (23b), (24b), (27) and (31) into Eq. (11), for  $dB(s) = J(\xi_s, \eta_s)d\eta_s$ , integration along the real boundary ( $\xi_s = \xi_0$ ) of the elliptic hole yields

$$u_z^M(\xi_x, \eta_x) = \frac{S}{\mu} c e^{-\xi_x} \sin \eta_x \cosh \xi_0 (\cosh \xi_0 + \sinh \xi_0), \quad x = (\xi_x, \eta_x) \in D. \tag{32}$$

By substituting Eqs. (7) and (32) into Eq. (8), we have the total displacement

$$u_z(\xi_x, \eta_x) = \frac{S}{\mu} c \sin \eta_x (\sinh \xi_x + e^{\xi_0 - \xi_x} \cosh \xi_0). \tag{33}$$

Now, we consider an elliptic hole in an infinite elastic body under the remote anti-plane shear stress in the different direction ( $\sigma_{yz}^\infty = 0$  and  $\sigma_{xz}^\infty = S$ ) as shown in Fig. 6. In this case, we follow the similar solving procedure, and we have the total displacement

$$u_z(\xi_x, \eta_x) = \frac{S}{\mu} c \cos \eta_x (\cosh \xi_x + e^{\xi_0 - \xi_x} \sinh \xi_0). \tag{34}$$

After comparing Eqs. (33) with (34), not only  $\sin \eta_x$  but also  $\sinh \xi_x$  and  $\cosh \xi_0$  are all changed to  $\cos \eta_x$ ,  $\cosh \xi_x$  and  $\sinh \xi_0$ , respectively.

### 3 Analytical solution of an infinite elastic body containing circular rigid inclusion or an elliptic rigid inclusion under the remote anti-plane shear by using the degenerate kernel

#### 3.1 A circular rigid inclusion under the remote anti-plane shear ( $\sigma_{yz}^\infty = S$ and $\sigma_{xz}^\infty = 0$ ) and ( $\sigma_{yz}^\infty = 0$ and $\sigma_{xz}^\infty = S$ )

In the case of rigid inclusion, the solution procedure of the total displacement is the same as the hole but different boundary condition (Neumann to Dirichlet). Now, we consider a circular rigid inclusion in an infinite elastic body under the remote anti-plane shear stress ( $\sigma_{yz}^\infty = S$  and  $\sigma_{xz}^\infty = 0$ ) as shown in Fig. 7. (Since the inclusion is rigid, taking free body of only inclusion is omitted.)

Rigid inclusion yields the Dirichlet boundary condition,

$$u_z(x) = 0, \quad x \in B. \tag{35}$$

The stress and displacement at infinity give

$$\sigma_{yz}^\infty = S, \quad |y| \rightarrow \infty, \quad \text{and} \quad u_z^\infty = \frac{Sy}{\mu}, \quad |y| \rightarrow \infty, \tag{36}$$

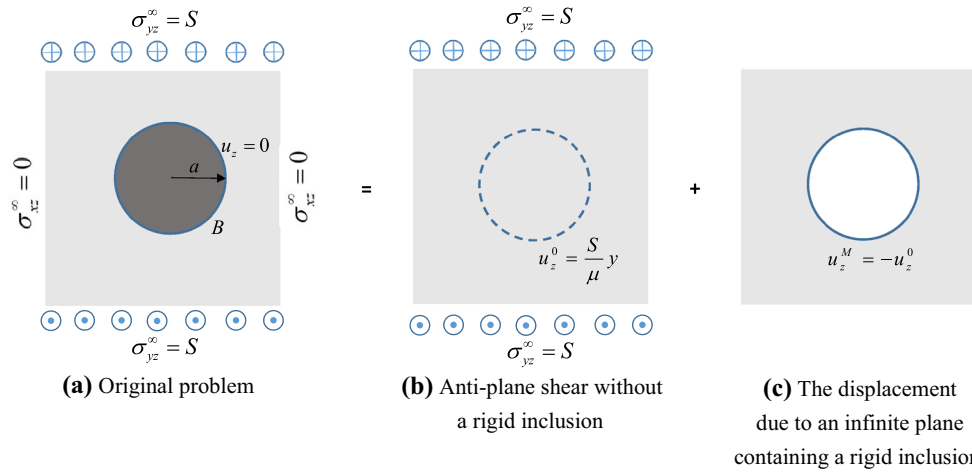


**Fig. 7** A circular rigid inclusion in an infinite elastic body under the remote anti-plane shear loading ( $\sigma_{yz}^\infty = S$  and  $\sigma_{xz}^\infty = 0$ )

respectively. Since  $u_z^\infty$  is given in Eq. (36), the displacement along the circular boundary in the infinite plane without a rigid inclusion is

$$u_z^0(s) = \frac{S}{\mu} R \sin \theta, \quad s = (R, \theta) \in B, \tag{37}$$

in polar coordinates. The specified boundary data  $u_z^M(s)$  along the circular boundary yield

$$u_z^M(s) = -u_z^0 = -\frac{S}{\mu} R \sin \theta, \quad s = (R, \theta) \in B, \tag{38}$$

By applying the Fourier expansions, the unknown boundary density  $t^M(s)$  can be expressed by

$$t^M(s) = a_0 + \sum_{n=1}^{\infty} a_n \cos n\theta + \sum_{n=1}^{\infty} b_n \sin n\theta, \quad 0 \leq \theta < 2\pi, \quad s = (R, \theta) \in B, \tag{39}$$

where  $a_0$ ,  $a_n$  and  $b_n$  are the unknown coefficients of Fourier series to be determined. By substituting Eqs. (9a), (10a), (38), and (39) into Eq. (12), for  $dB(s) = a d\theta (R = a)$  and locating  $x$  on the real boundary ( $\rho = a$ ) for the circular rigid inclusion, we have

$$2\pi a \ln a a_0 - \sum_{n=1}^{\infty} \frac{1}{n} a\pi \cos(n\phi) a_n + \sum_{n=1}^{\infty} \frac{1}{n} a\pi \sin(n\phi) b_n = \frac{S}{\mu} a\pi \sin(\phi), \quad x = (\xi_x, \eta_x) \in B, \tag{40}$$

where  $x$  can be in the domain or on the boundary since a proper degenerate kernel is already chosen. After comparing coefficients of the basis,  $1, \cos n\phi$  and  $\sin n\phi$ , we have

$$\begin{cases} (2 \ln a) a_0 = 0, & n = 0, \\ a_n = 0, & n = 1, 2, 3, \dots, \\ b_1 = \frac{S}{\mu}, & n = 1, \\ b_n = 0, & n = 2, 3, \dots \end{cases} \tag{41}$$

In Eq. (41),  $a_0$  can be determined if  $\ln a \neq 0$ . The coefficient of  $a_0$  can be arbitrary which results in a nonunique solution problem once  $a$  is equal to one. This indicates the occurring mechanism of the degenerate scale in the BEM/BIEM due to the  $\ln r$  kernel in conjunction with the Dirichlet B.C. of rigid inclusion. Therefore, Eq. (39) can be written as

$$t^M(s) = \frac{S}{\mu} \sin \theta, \quad s = (R, \theta) \in B. \tag{42}$$

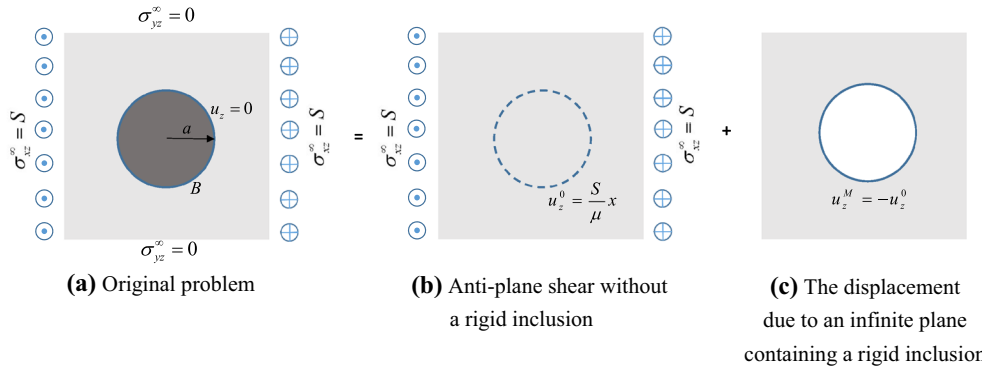


**Fig. 8** A circular rigid inclusion in an infinite elastic body under the remote anti-plane shear loading ( $\sigma_{yz}^\infty = 0$  and  $\sigma_{xz}^\infty = S$ )

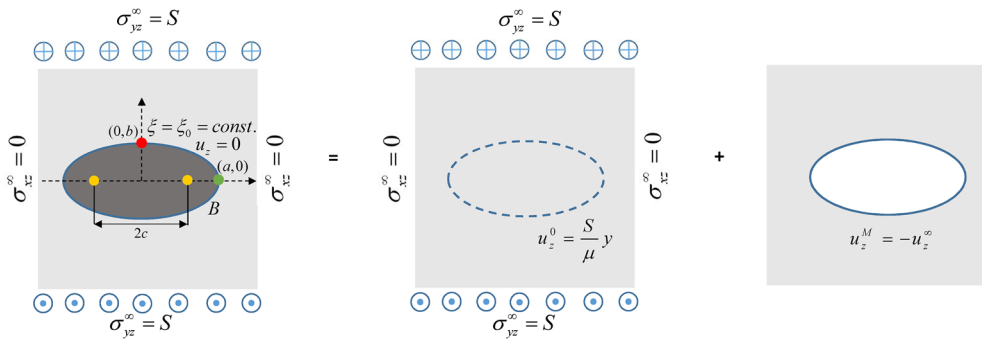


**Fig. 9** An elliptic rigid inclusion in an infinite elastic body under the remote anti-plane shear loading ( $\sigma_{yz}^\infty = S$  and  $\sigma_{xz}^\infty = 0$ )

By substituting Eqs. (9b), (10b), (38) and (42) into Eq. (11), for  $dB(s) = ad\theta$ , integration along on the real boundary ( $R = a$ ) yields

$$u_z^M(\rho, \phi) = -\frac{S a^2}{\mu \rho} \sin \phi, \quad x = (\rho, \phi) \in D. \tag{43}$$

By substituting Eqs. (36) and (43) into Eq. (8), we have

$$u_z(\rho, \phi) = \frac{S}{\mu} \rho \left( 1 - \frac{a^2}{\rho^2} \right) \sin \phi. \tag{44}$$

The total displacement expressed in the polar coordinates can be obtained in Eq. (44). For the circular rigid inclusion in the different direction ( $\sigma_{yz}^\infty = 0$  and  $\sigma_{xz}^\infty = S$ ) as shown in Fig. 8, the total displacement can be obtained by replacing  $\phi$  to  $\phi + \pi/2$  in Eq. (44) as

$$u_z(\rho, \phi) = \frac{S}{\mu} \rho \left( 1 - \frac{a^2}{\rho^2} \right) \cos \phi. \tag{45}$$

**3.2 An elliptic rigid inclusion under the remote anti-plane shear ( $\sigma_{yz}^\infty = S$  and  $\sigma_{xz}^\infty = 0$ ) and ( $\sigma_{yz}^\infty = 0$  and  $\sigma_{xz}^\infty = S$ )**

Now, we consider an elliptic rigid inclusion in an infinite elastic body under the remote anti-plane shear stress ( $\sigma_{yz}^\infty = S$  and  $\sigma_{xz}^\infty = 0$ ) as shown in Fig. 9. (Since the inclusion is rigid, taking free body of only inclusion is omitted.)

Since  $u_z^\infty$  is given in Eq. (36), the displacement along the elliptic boundary in the infinite plane without a rigid inclusion is

$$u_z^0(s) = \frac{S}{\mu} c \sinh \xi_s \sin \eta_s, \quad s = (\xi_s, \eta_s) \in B, \tag{46}$$

in elliptic coordinates. The specified boundary data  $u_z^M(s)$  along the elliptic boundary yield

$$u_z^M(s) = -u^0(s) = -\frac{S}{\mu} c \sinh \xi_s \sin \eta_s, \quad s = (\xi_s, \eta_s) \in B, \tag{47}$$

respectively. By applying the Fourier expansions, the unknown boundary density  $t^M(s)$  can be expressed by

$$t^M(s) = \frac{1}{J_s} (a_0 + \sum_{n=1}^{\infty} a_n \cos n\eta_s + \sum_{n=1}^{\infty} b_n \sin n\eta_s), \quad 0 \leq \eta_s < 2\pi, \quad s = (\xi_s, \eta_s) \in B, \tag{48}$$

where  $a_0$ ,  $a_n$  and  $b_n$  are the unknown coefficients of Fourier series to be determined. By substituting Eqs. (23a), (24a), (47) and (48) into Eq. (12), for  $dB(s) = J(\xi_s, \eta_s)d\eta_s$  ( $\xi_s = \xi_0$ ) and locating  $x$  on the real boundary ( $\xi_x = \xi_0$ ) for the elliptic rigid inclusion, we have

$$\begin{aligned} & (\xi_0 + \ln \frac{c}{2})2\pi a_0 - \sum_{n=1}^{\infty} \frac{2}{n}\pi e^{-n\xi_0} \cosh n\xi_0 \cos n\eta_x a_n - \sum_{n=1}^{\infty} \frac{2}{n}\pi e^{-n\xi_0} \sinh n\xi_0 \sin n\eta_x b_n \\ & = 2\pi \frac{S}{\mu} c e^{-\xi_0} \sinh \xi_0 \sin \eta_x, \quad x = (\xi_x, \eta_x) \in B. \end{aligned} \tag{49}$$

After comparing coefficients of the basis, 1,  $\cos n\eta_x$  and  $\sin n\eta_x$ , we have

$$\begin{cases} (\xi_0 + \ln \frac{c}{2})a_0 = 0, & n = 0, \\ a_n = 0, & n = 1, 2, 3, \dots, \\ b_1 = -\frac{S}{\mu} c \sinh \xi_0, & n = 1, \\ b_n = 0, & n = 2, 3, \dots. \end{cases} \tag{50}$$

In Eq. (50),  $a_0$  can be determined if  $\xi_0 + \ln(c/2) \neq 0$ . The coefficient of  $a_0$  can be arbitrary which results in a nonunique solution problem once  $a + b = 2$ . This also indicates the occurring mechanism of the degenerate scale in the BEM/BIEM due to the  $\ln r$  kernel in conjunction with the Dirichlet B.C. of rigid inclusion. Therefore, Eq. (48) can be written as

$$t^M(s) = \frac{-1}{J_s} \frac{S}{\mu} c \sinh \xi_0 \sin \eta_s, \quad s = (\xi_s, \eta_s) \in B. \tag{51}$$

By substituting Eqs. (23b), (24b), (47) and (51) into Eq. (11), for  $dB(s) = J(\xi_s, \eta_s)d\eta_s$ , integration along the real boundary ( $\xi_s = \xi_0$ ) of the elliptic rigid inclusion yields

$$u_z^M(\xi_x, \eta_x) = -\frac{S}{\mu} c e^{\xi_0 - \xi_x} \sin \eta_x \sinh \xi_0, \quad x = (\xi_x, \eta_x) \in D. \tag{52}$$

By substituting Eqs. (36) and (52) into Eq. (8), we have the total displacement,

$$u_z(\xi_x, \eta_x) = \frac{S}{\mu} c \sin \eta_x (\sinh \xi_x - e^{\xi_0 - \xi_x} \sinh \xi_0). \tag{53}$$

Now, we consider an elliptic rigid inclusion in an infinite elastic body under the remote anti-plane shear stress in the different direction ( $\sigma_{yz}^\infty = 0$  and  $\sigma_{xz}^\infty = S$ ) as shown in Fig. 10. (Since the inclusion is rigid, taking free body of only inclusion is omitted.) We have the total displacement,

$$u_z(\xi_x, \eta_x) = \frac{S}{\mu} c \cos \eta_x (\cosh \xi_x - e^{\xi_0 - \xi_x} \cosh \xi_0). \tag{54}$$

After comparing Eq. (53) with Eq. (54), not only  $\sin \eta_x$  but also  $\sinh \xi_x$  and  $\sinh \xi_0$  are all changed to  $\cos \eta_x$ ,  $\cosh \xi_x$  and  $\cosh \xi_0$ , respectively.

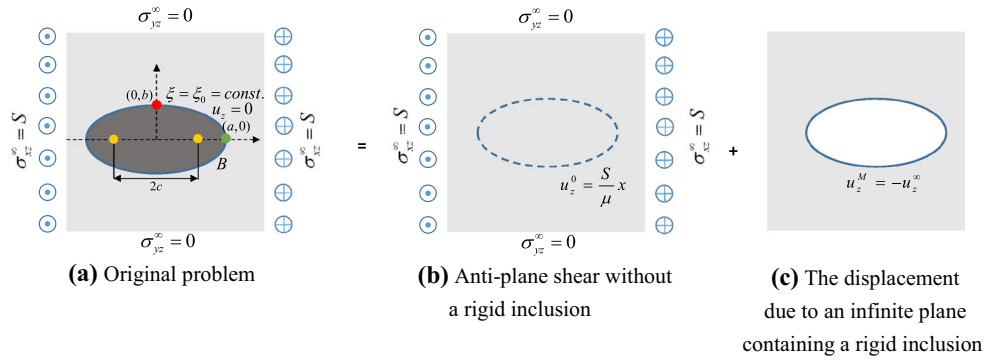


**Fig. 10** An elliptic rigid inclusion in an infinite elastic body under the remote anti-plane shear loading ( $\sigma_{yz}^{\infty} = 0$  and  $\sigma_{xz}^{\infty} = S$ )

#### 4 SCFs

Since the total displacement is obtained in the previous section, stresses can be easily determined. SCF is defined as

$$\text{SCF} = \frac{\sqrt{(\sigma_{xz})^2 + (\sigma_{yz})^2}}{\sigma^{\infty}} = \frac{|\tau|}{\sigma^{\infty}}, \quad (55)$$

where  $\tau$  is the circumferential shear stress along the boundary of the hole or the rigid inclusion and  $\sigma^{\infty}$  is the remote shear. The equivalence between  $\sqrt{(\sigma_{xz})^2 + (\sigma_{yz})^2}$  and  $|\tau|$  can be derived by using invariants of tensor. The eigenvalue of  $\lambda$  for the stress tensor  $\sigma_{ij}$  can be determined by

$$\det(\sigma_{ij} - \lambda \delta_{ij}) = 0. \quad (56)$$

We find the invariant  $I$ ,

$$I = (\sigma_{13})^2 + (\sigma_{23})^2. \quad (57)$$

By employing the transformation law of the second-order tensor in the component form like a Mohr circle, we have

$$\bar{\sigma}_{pq} = l_{pi} l_{qj} \sigma_{ij}. \quad (58)$$

By rotating the coordinates with respect to the  $x_3$  axis, we have  $\bar{x}_1$  in the normal vector  $n$  and  $\bar{x}_2$  in the tangent vector  $m$  as shown in Figs. 11 and 12, we have

$$\bar{\sigma}_{n3} = l_{ni} l_{3j} \sigma_{ij}, \quad (59)$$

and

$$\bar{\sigma}_{m3} = l_{mi} l_{3j} \sigma_{ij}. \quad (60)$$

Therefore,  $\bar{\sigma}_{n3}$  reduces to

$$\bar{\sigma}_{n3} = l_{n1} l_{33} \sigma_{13} + l_{n2} l_{33} \sigma_{23} = \cos(\alpha) \sigma_{13} + \sin(\alpha) \sigma_{23} \quad (61)$$

while  $\bar{\sigma}_{m3}$  reduces to

$$\bar{\sigma}_{m3} = l_{m1} l_{33} \sigma_{13} + l_{m2} l_{33} \sigma_{23} = -\sin(\alpha) \sigma_{13} + \cos(\alpha) \sigma_{23} \quad (62)$$

By comparing Eqs. (57), (61) and (62), we have

$$(\bar{\sigma}_{n3})^2 + (\bar{\sigma}_{m3})^2 = (\sigma_{13})^2 + (\sigma_{23})^2. \quad (63)$$

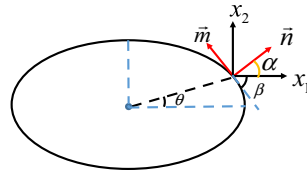


**Fig. 11** The normal vector  $n$  and tangent vector  $m$  along the boundary,  $\vec{n} = (n_1, n_2) = (\cos(\alpha), \sin(\alpha))$ ,  $\vec{m} = (-n_2, n_1) = (-\sin(\alpha), \cos(\alpha))$

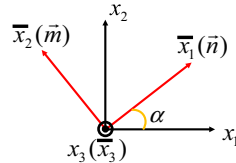


**Fig. 12** Two observer systems for the stress tensor

According to the traction-free of the Neumann boundary condition,  $\bar{\sigma}_{n3}$  is found to be zero. Therefore, Eq. (63) is simplified to,

$$\bar{\sigma}_{m3} = \tau = \sqrt{(\sigma_{13})^2 + (\sigma_{23})^2}. \tag{64}$$

It is interesting to find that Eq. (64) indicates shear stress along the boundary for the hole, while Eq. (63) changes to

$$\bar{\sigma}_{n3} = \tau = \sqrt{(\sigma_{13})^2 + (\sigma_{23})^2}, \tag{65}$$

for the rigid inclusion. Equations (64) and (65) provide us expressions for the SCF of a hole or a rigid inclusion, respectively. This can help us to determine the SCF faster than the general formula although the general formula can also determine the SCF.

Here, we demonstrated two methods to solve the SCF.

Method 1: General formula  $SCF = \frac{\sqrt{(\sigma_{xz})^2 + (\sigma_{yz})^2}}{\sigma^\infty}$

Based on the analytical displacement of the total field derived by using the degenerate kernel in terms of polar coordinates  $(\rho, \phi)$ , the Cartesian components of the position vector are

$$x = \rho \cos \phi, \tag{66}$$

$$y = \rho \sin \phi. \tag{67}$$

For a circular hole under the remote anti-plane loading  $\sigma_{yz}^\infty = S$ ,  $\sigma_{xz}^\infty = 0$ , the general formula yields

$$SCF = \frac{\left| \mu \sqrt{\left( \frac{\partial u_z}{\partial \rho} \cos \phi - \frac{\sin \phi}{\rho} \frac{\partial u_z}{\partial \phi} \right)^2 + \left( \frac{\partial u_z}{\partial \rho} \sin \phi + \frac{\cos \phi}{\rho} \frac{\partial u_z}{\partial \phi} \right)^2} \right|}{\sigma^\infty}. \tag{68}$$

By substituting Eq. (21) into Eq. (68) for  $\rho = a$ , the maximum SCF occurs at  $\phi = 0$  or  $\pi$ ,

$$SCF = \frac{|2S \cos \phi|}{S} = 2. \tag{69}$$

For the case of the remote anti-plane loading  $\sigma_{yz}^\infty = 0$ ,  $\sigma_{xz}^\infty = S$ , the maximum SCF occurs at  $\phi = \frac{1}{2}\pi$  or  $\frac{3}{2}\pi$ ,

$$SCF = \frac{|2S \sin \phi|}{S} = 2. \tag{70}$$

Equations (69) and (70) show the SCF of a circular hole in an infinite elastic body under the remote anti-plane shear  $\sigma_{yz}^\infty = S$ ,  $\sigma_{xz}^\infty = 0$  and  $\sigma_{yz}^\infty = 0$ ,  $\sigma_{xz}^\infty = S$ , respectively. For the circular rigid inclusion under the remote anti-plane loading  $\sigma_{yz}^\infty = S$ ,  $\sigma_{xz}^\infty = 0$ , we have the maximum SCF o occurs at  $\phi = \frac{1}{2}\pi$  or  $\frac{3}{2}\pi$ ,

$$SCF = \frac{|2S \sin \phi|}{S} = 2, \tag{71}$$

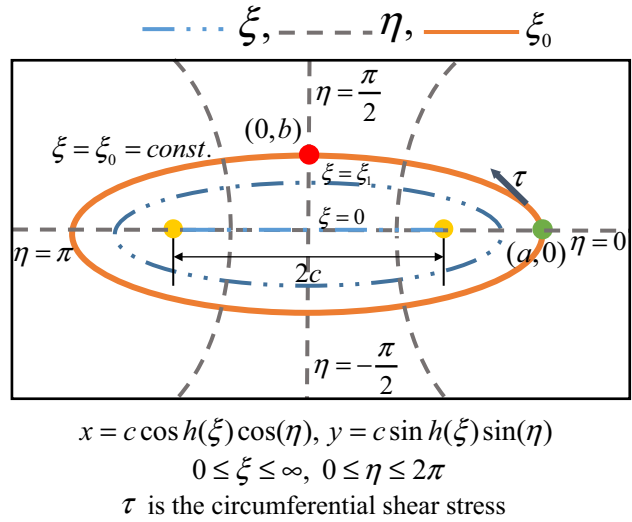


**Fig. 13** The elliptic coordinates

and the maximum SCF occurs at  $\phi = 0$  or  $\pi$ ,

$$SCF = \frac{|2S \cos \phi|}{S} = 2, \tag{72}$$

under the remote anti-plane loading  $\sigma_{yz}^\infty = 0, \sigma_{xz}^\infty = S$ , respectively.

In elliptic coordinates  $(\xi, \eta)$  for the elliptic case as shown in Fig. 13, the Cartesian components of the position vector are

$$x = c \cosh \xi \cos \eta, \tag{73}$$

$$y = c \sinh \xi \sin \eta, \tag{74}$$

where the curve of  $\xi = \text{constant}$  is the elliptic boundary of the hole or rigid inclusion and the curve of  $\eta = \text{constant}$  is portion of hyperbolae all having the same foci  $(\pm c, 0)$ .

Therefore, the SCF of an elliptic hole yields the general formula,

$$SCF = \frac{\left| \mu \sqrt{\left( h_1 \frac{\partial u_z}{\partial \xi_x} - h_2 \frac{\partial u_z}{\partial \eta_x} \right)^2 + \left( h_2 \frac{\partial u_z}{\partial \xi_x} + h_1 \frac{\partial u_z}{\partial \eta_x} \right)^2} \right|}{\sigma^\infty}, \tag{75}$$

where  $h_1 = \frac{\sinh \xi_x \cos \eta_x}{c((\sinh \xi_x \cos \eta_x)^2 + (\cosh \xi_x \sin \eta_x)^2)}$ , and  $h_2 = \frac{\cosh \xi_x \sin \eta_x}{c((\sinh \xi_x \cos \eta_x)^2 + (\cosh \xi_x \sin \eta_x)^2)}$ .

By substituting Eq. (33) into Eq. (75), for  $\xi_x = \xi_0$ , we have

$$SCF = \sqrt{\frac{2e^{2\xi_0} \cos^2 \eta_x}{\cosh 2\xi_0 - \cos 2\eta_x}}, \tag{76}$$

By substituting  $\eta_x = 0$  or  $\pi$  into Eq. (76), for  $\xi_0 = \tanh^{-1}(\frac{b}{a}) = \frac{1}{2} \ln(\frac{a+b}{a-b})$ , we have

$$SCF = \frac{2}{1 - e^{-2\xi_0}} = 1 + \frac{1}{k}, \tag{77}$$

where  $k = b/a$  is the aspect ratio of the ellipse. By substituting Eq. (34) into Eq. (75), for  $\xi_x = \xi_0$  with respect to the loading  $\sigma_{yz}^\infty = 0, \sigma_{xz}^\infty = S$ , we have

$$SCF = \sqrt{\frac{2e^{2\xi_0} \sin^2 \eta_x}{\cosh 2\xi_0 - \cos 2\eta_x}}, \tag{78}$$

By substituting  $\eta_x = \frac{\pi}{2}$  or  $\frac{3\pi}{2}$  into Eq. (78), for  $\xi_0 = \tanh^{-1}(\frac{b}{a}) = \frac{1}{2} \ln(\frac{a+b}{a-b})$ , we have

$$\text{SCF} = \frac{2}{1 + e^{-2\xi_0}} = 1 + k. \tag{79}$$

Equations (77) and (79) show the SCF of an elliptic hole in an infinite elastic body under the remote anti-plane shear of  $\sigma_{yz}^\infty = S$ ,  $\sigma_{xz}^\infty = 0$  and  $\sigma_{yz}^\infty = 0$ ,  $\sigma_{xz}^\infty = S$ , respectively. For the elliptic rigid inclusion under the remote anti-plane loading  $\sigma_{yz}^\infty = S$ ,  $\sigma_{xz}^\infty = 0$ , the maximum SCF occurs at  $\eta_x = \frac{\pi}{2}$  or  $\frac{3\pi}{2}$  and yields

$$\text{SCF} = \frac{2}{1 + e^{-2\xi_0}} = 1 + k. \tag{80}$$

For the remote anti-plane loading  $\sigma_{yz}^\infty = 0$  and  $\sigma_{xz}^\infty = S$ , the maximum SCF occurs at  $\eta_x = 0$  or  $\pi$  and yields

$$\text{SCF} = \frac{2}{1 - e^{-2\xi_0}} = 1 + \frac{1}{k}. \tag{81}$$

These SCFs of circular/elliptic hole or rigid inclusion also yield the same result as mentioned in [12,14]. When  $k$  approaches one (a circular hole), the SCF value tends to the value 2 as in [9,10,12,14,26].

Method 2: The present formula  $\text{SCF} = \frac{|\tau|}{\sigma^\infty}$

One of the reason that we employ the degenerate kernel in terms of polar coordinates or elliptic coordinates is that we can own its benefits. By employing the transformation law of the  $2^{nd}$  order tensor, we found that only taking the tangential derivative or the normal derivative of the total displacement and multiplying  $\mu$  can obtain  $\tau$ . For the circular hole, the tangential derivative multiplying  $\mu$  yields

$$\tau = \frac{\mu}{\rho} \frac{\partial u_z}{\partial \phi}, \tag{82}$$

in polar coordinates. For the elliptic hole, we have

$$\tau = \frac{\mu}{h} \frac{\partial u_z}{\partial \eta_x}, \tag{83}$$

where  $h = c\sqrt{\sinh^2(\xi_x) + \sin^2(\eta_x)}$  in elliptic coordinates. The case of the rigid inclusion yields the normal derivative and multiplying  $\mu$  yields

$$\tau = \mu \frac{\partial u_z}{\partial \rho}, \tag{84}$$

in polar coordinates for the circular case, while the elliptic rigid inclusion yields

$$\tau = \frac{\mu}{h} \frac{\partial u_z}{\partial \xi_x}, \tag{85}$$

in elliptic coordinates. Figure 13 also shows the definition of  $\tau$  in our system.

The formula of the present approach is simpler to calculate the SCF than the general way. Therefore, we can efficiently calculate the value of SCF for the hole and rigid inclusion cases. The comparison of a circular hole and rigid inclusion under the remote anti-plane shear by using the degenerate kernel is shown in Table 1. The comparison of an elliptic hole and a rigid inclusion under the remote anti-plane shear by using the degenerate kernel is shown in Table 2. It is interesting that the result shows that the SCF values for hole and rigid inclusions are the same, but the loadings are switched as the [10] mentioned. The reciprocal relation can be understood as the general Cauchy–Riemann formula in terms of the tangent derivative and the normal derivative on the boundary in the present result. It indicates that we can derive an analytic function that its real part and imaginary part are the total displacement of the rigid inclusion and hole but rely on its loading, respectively, as shown in Tables 3 and 4. Not only the benefits by using the degenerate kernel we have, but also the phenomenon we can observe without using the complex variables. Besides, the occurring mechanism of the degenerate scale in the BEM/BIEM for the rigid inclusion case is well captured.

**Table 1** The comparison of results for a circular hole and a rigid inclusion in an infinite elastic body under the remote anti-plane shear  $\sigma_{yz}^\infty = S$ ,  $\sigma_{xz}^\infty = 0$  and  $\sigma_{yz}^\infty = 0$ ,  $\sigma_{xz}^\infty = S$  by using the degenerate kernel

Relation	The reciprocal relation		The reciprocal relation		
Figure sketch					
Coordinates	Polar coordinates				
Degenerate kernel	$U(\mathbf{s}, \mathbf{x}) = \begin{cases} U^i(R, \theta; \rho, \phi) = \ln R - \sum_{m=1}^{\infty} \frac{1}{m} \left(\frac{\rho}{R}\right)^m \cos m(\theta - \phi), & R \geq \rho, \\ U^e(R, \theta; \rho, \phi) = \ln \rho - \sum_{m=1}^{\infty} \frac{1}{m} \left(\frac{R}{\rho}\right)^m \cos m(\theta - \phi), & \rho > R. \end{cases}$		$T(\mathbf{s}, \mathbf{x}) = \begin{cases} T^i(R, \theta; \rho, \phi) = -\left(\frac{1}{R} + \sum_{m=1}^{\infty} \left(\frac{\rho^m}{R^{m+1}}\right) \cos m(\theta - \phi)\right), & R > \rho, \\ T^e(R, \theta; \rho, \phi) = \sum_{m=1}^{\infty} \left(\frac{R^{m-1}}{\rho^m}\right) \cos m(\theta - \phi), & \rho > R. \end{cases}$		
Boundary condition	$t(x) = \frac{\partial u_z}{\partial n} = 0, x \in B$	$u_z(x) = 0, x \in B$	$t(x) = \frac{\partial u_z}{\partial n} = 0, x \in B$	$u_z(x) = 0, x \in B$	
Stress and displacement at infinity	$\sigma_{yz}^\infty = S,  y  \rightarrow \infty$ $u_z^\infty = \frac{Sy}{\mu},  y  \rightarrow \infty$	$\sigma_{xz}^\infty = S,  x  \rightarrow \infty$ $u_z^\infty = \frac{Sx}{\mu},  x  \rightarrow \infty$	$\sigma_{xz}^\infty = S,  x  \rightarrow \infty$ $u_z^\infty = \frac{Sx}{\mu},  x  \rightarrow \infty$	$\sigma_{yz}^\infty = S,  y  \rightarrow \infty$ $u_z^\infty = \frac{Sy}{\mu},  y  \rightarrow \infty$	
Total displacement $u_z(\rho, \phi)$	$u_z(\rho, \phi) = \frac{S}{\mu} \rho \left(1 + \frac{a^2}{\rho^2}\right) \sin \phi$	$u_z(\rho, \phi) = \frac{S}{\mu} \rho \left(1 - \frac{a^2}{\rho^2}\right) \cos \phi$	$u_z(\rho, \phi) = \frac{S}{\mu} \rho \left(1 + \frac{a^2}{\rho^2}\right) \cos \phi$	$u_z(\rho, \phi) = \frac{S}{\mu} \rho \left(1 - \frac{a^2}{\rho^2}\right) \sin \phi$	
$\tau$	$\sqrt{(\sigma_{xz}^\infty)^2 + (\sigma_{yz}^\infty)^2}$	$2S \cos \phi$	$2S \cos \phi$	$2S \sin \phi$	$2S \sin \phi$
	$\tau^m = \frac{\partial u_z}{\partial m} = \frac{\mu}{\rho} \frac{\partial u_z}{\partial \phi}$	$2S \cos \phi$	0	$-2S \sin \phi$	0
	$\tau^n = \frac{\partial u_z}{\partial n} = \mu \frac{\partial u_z}{\partial \rho}$	0	$2S \cos \phi$	0	$2S \sin \phi$
SCF	$\frac{\sqrt{(\sigma_{xz}^\infty)^2 + (\sigma_{yz}^\infty)^2}}{\sigma^\infty}$	$ 2 \cos \phi $	$ 2 \cos \phi $	$ 2 \sin \phi $	$ 2 \sin \phi $
	$\frac{ \tau^m }{\sigma^\infty}$ or $\frac{ \tau^n }{\sigma^\infty}$	$ 2 \cos \phi $	$ 2 \cos \phi $	$ -2 \sin \phi $	$ 2 \sin \phi $

**5 Illustration of examples and discussions**

To verify our result, we compared with the formula in Lubarda’s paper [14]. In the present method, we do not need to derive the relation of the angles,  $\beta$  and  $\theta$  as shown in Fig. 11. We only need take the tangential or the normal derivative with respect to the total displacement along the boundary. Then, the SCFs can be easily determined. The variation of the circumferential stresses  $\tau$  and  $\tau^\infty$  under the remote shear  $\sigma_{yz}^\infty = \sigma_{xz}^\infty = \sigma^\infty$  is shown in Fig. 14, where  $\tau^\infty = \frac{\mu}{\rho} \frac{\partial u_z^\infty}{\partial \eta_x}$ . The elastic strain energy density  $U$  is defined as the strain energy per unit volume as shown below [14]:

$$U = \tau^2 / 2\mu, \tag{86}$$

while the elastic strain energy along the elliptic boundary in the infinite plane without a hole is

$$U^\infty = \left( (\sigma_{yz}^\infty)^2 + (\sigma_{xz}^\infty)^2 \right) / 2\mu. \tag{87}$$

**Table 2** The comparison of results for an elliptic hole and a rigid inclusion in an infinite elastic body under the remote anti-plane shear  $\sigma_{yz}^\infty = S$ ,  $\sigma_{xz}^\infty = 0$  and  $\sigma_{yz}^\infty = 0$ ,  $\sigma_{xz}^\infty = S$  by using the degenerate kernel

Relation	The reciprocal relation		The reciprocal relation	
Figure sketch				
Coordinates	Elliptic coordinates			
Degenerate kernel	$U^I(\xi_s, \eta_s; \xi_x, \eta_x) = \xi_x + \ln \frac{c}{2} - \sum_{m=1}^{\infty} \frac{2}{m} e^{-m\xi_s} \cosh m\xi_x \cos m\eta_x \cos m\eta_s - \sum_{m=1}^{\infty} \frac{2}{m} e^{-m\xi_s} \sinh m\xi_x \sin m\eta_x \sin m\eta_s, \quad \xi_x > \xi_s,$ $U^E(\xi_s, \eta_s; \xi_x, \eta_x) = \xi_x + \ln \frac{c}{2} - \sum_{m=1}^{\infty} \frac{2}{m} e^{-m\xi_s} \cosh m\xi_x \cos m\eta_x \cos m\eta_s - \sum_{m=1}^{\infty} \frac{2}{m} e^{-m\xi_s} \sinh m\xi_x \sin m\eta_x \sin m\eta_s, \quad \xi_x < \xi_s,$ $T^I(\xi_s, \eta_s; \xi_x, \eta_x) = \frac{-1}{J(\xi_s, \eta_s)} \left( 1 + 2 \sum_{m=1}^{\infty} e^{-m\xi_s} \cosh m\xi_x \cos m\eta_x \cos m\eta_s + 2 \sum_{m=1}^{\infty} e^{-m\xi_s} \sinh m\xi_x \sin m\eta_x \sin m\eta_s \right), \quad \xi_s > \xi_x,$ $T^E(\xi_s, \eta_s; \xi_x, \eta_x) = \frac{1}{J(\xi_s, \eta_s)} \left( 2 \sum_{m=1}^{\infty} e^{-m\xi_s} \sinh m\xi_x \cos m\eta_x \cos m\eta_s + 2 \sum_{m=1}^{\infty} e^{-m\xi_s} \cosh m\xi_x \sin m\eta_x \sin m\eta_s \right), \quad \xi_s < \xi_x.$			
Boundary condition	$t(x) = \frac{\partial u_z}{\partial n} = 0, x \in B$	$u_z(x) = 0, x \in B$	$t(x) = \frac{\partial u_z}{\partial n} = 0, x \in B$	$u_z(x) = 0, x \in B$
Stress and displacement at infinity	$\sigma_{yz}^\infty = S,  y  \rightarrow \infty$	$\sigma_{yz}^\infty = S,  x  \rightarrow \infty$	$\sigma_{yz}^\infty = S,  x  \rightarrow \infty$	$\sigma_{yz}^\infty = S,  y  \rightarrow \infty$
	$u_z^\infty = \frac{S y}{\mu},  y  \rightarrow \infty$	$u_z^\infty = \frac{S x}{\mu},  x  \rightarrow \infty$	$u_z^\infty = \frac{S x}{\mu},  x  \rightarrow \infty$	$u_z^\infty = \frac{S y}{\mu},  y  \rightarrow \infty$
Total displacement $u_z(\xi_s, \eta_s)$	$\frac{S}{\mu} c \sin \eta_s (\sinh \xi_x + e^{\xi_0 - \xi_x} \cosh \xi_0)$	$\frac{S}{\mu} c \cos \eta_s (\cosh \xi_x - e^{\xi_0 - \xi_x} \cosh \xi_0)$	$\frac{S}{\mu} c \cos \eta_s (\cosh \xi_x + e^{\xi_0 - \xi_x} \sinh \xi_0)$	$\frac{S}{\mu} c \sin \eta_s (\sinh \xi_x - e^{\xi_0 - \xi_x} \sinh \xi_0)$
$\tau$	$\sqrt{(\sigma_{xz}^\infty)^2 + (\sigma_{yz}^\infty)^2}$	$Se^{\xi_0} \cos \eta_s \sqrt{\frac{2}{\cosh 2\xi_0 - \cos 2\eta_x}}$	$Se^{\xi_0} \cos \eta_s \sqrt{\frac{2}{\cosh 2\xi_0 - \cos 2\eta_x}}$	$Se^{\xi_0} \sin \eta_s \sqrt{\frac{2}{\cosh 2\xi_0 - \cos 2\eta_x}}$
	$\tau^m = \frac{\partial u_z}{\partial m} = \frac{\mu}{h} \frac{\partial u_z}{\partial \eta_x}$	$\frac{Se^{\xi_0} \cos \eta_s}{\sqrt{\sinh^2 \xi_0 + \sin^2 \eta_x}}$	0	$\frac{-Se^{\xi_0} \sin \eta_s}{\sqrt{\sinh^2 \xi_0 + \sin^2 \eta_x}}$
	$\tau^n = \frac{\partial u_z}{\partial n} = \frac{\mu}{h} \frac{\partial u_z}{\partial \xi_x}$	0	$\frac{Se^{\xi_0} \cos \eta_x}{\sqrt{\sinh^2 \xi_0 + \sin^2 \eta_x}}$	$\frac{Se^{\xi_0} \sin \eta_x}{\sqrt{\sinh^2 \xi_0 + \sin^2 \eta_x}}$
SCF	$\frac{\sqrt{(\sigma_{xz}^\infty)^2 + (\sigma_{yz}^\infty)^2}}{\sigma^\infty}$	$\left  e^{\xi_0} \cos \eta_s \sqrt{\frac{2}{\cosh 2\xi_0 - \cos 2\eta_x}} \right  *$	$\left  e^{\xi_0} \cos \eta_s \sqrt{\frac{2}{\cosh 2\xi_0 - \cos 2\eta_x}} \right $	$\left  e^{\xi_0} \sin \eta_s \sqrt{\frac{2}{\cosh 2\xi_0 - \cos 2\eta_x}} \right $
	$\left  \tau^m \right $ or $\left  \tau^n \right $	$\left  \frac{e^{\xi_0} \cos \eta_x}{\sqrt{\sinh^2 \xi_0 + \sin^2 \eta_x}} \right  **$	$\left  \frac{e^{\xi_0} \cos \eta_s}{\sqrt{\sinh^2 \xi_0 + \sin^2 \eta_x}} \right $	$\left  \frac{-e^{\xi_0} \sin \eta_x}{\sqrt{\sinh^2 \xi_0 + \sin^2 \eta_x}} \right $
$* = \sqrt{\frac{2}{(\cosh(2\xi_0) - \cos(2\eta_x))}} = \sqrt{\frac{2}{\left(\frac{e^{2\xi_0} + e^{-2\xi_0}}{2} - \cos(2\eta_x)\right)}} = \sqrt{\frac{4}{(e^{2\xi_0} + e^{-2\xi_0} - 2\cos(2\eta_x))}} \quad ** = \sqrt{\frac{1}{\left(\frac{e^{\xi_0} - e^{-\xi_0}}{2}\right)^2 + \frac{1 - \cos(2\eta_x)}{2}}} = \sqrt{\frac{4}{(e^{2\xi_0} - e^{-2\xi_0} - 2\cos(2\eta_x))}} \Rightarrow ***$				

The variation of  $U/U^\infty$  along the boundary of the ellipse versus  $k$ , under the loading of  $\sigma_{yz}^\infty \neq 0$ ,  $\sigma_{xz}^\infty = 0$ , is shown in Fig. 15. Figure 16 shows the variation of  $U/U^\infty$  along the boundary of the ellipse in the case when the loading is  $\sigma_{xz}^\infty = \sigma_{yz}^\infty$  and  $\sigma_{xz}^\infty = -\sigma_{yz}^\infty$ .

Four aspect ratios of  $k$  are considered. Both figures agree well with those of [14]. When we have the displacement field solution in an infinite elastic body with an elliptic hole under the remote anti-plane loading  $\sigma_{yz}^\infty = S$ ,  $\sigma_{xz}^\infty = 0$  and  $\sigma_{yz}^\infty = 0$ ,  $\sigma_{xz}^\infty = S$ , the displacement field solution of inclined elliptic hole or rigid

**Table 3** The Cauchy–Riemann relation between the circular hole and rigid inclusion with respect to different loading.

Relation	The reciprocal relation		The reciprocal relation	
Figure				
Function				
B.C.	$t(\nu) = \frac{\partial u_z}{\partial n} = 0, \nu \in B$	$u_z(\nu) = 0, \nu \in B$	$t(\nu) = \frac{\partial u_z}{\partial n} = 0, \nu \in B$	$u_z(\nu) = 0, \nu \in B$
Remote anti-plane shear	$\sigma_{xz}^\infty = S,  y  \rightarrow \infty$	$\sigma_{xz}^\infty = S,  x  \rightarrow \infty$	$\sigma_{xz}^\infty = S,  x  \rightarrow \infty$	$\sigma_{xz}^\infty = S,  y  \rightarrow \infty$
Analytic function $f(z) = u(x, y) + iv(x, y)$ $z = x + iy$	$f(z) = \frac{S}{\mu} \left( z - \frac{a^2}{z} \right)$		$f(z) = \frac{S}{\mu} \left( z + \frac{a^2}{z} \right)$	
$u = \text{Re}(f(z))$		Total displacement $u_z$ $\frac{S}{\mu} \left( \rho \cos \phi - \frac{a^2}{\rho} \cos \phi \right)$	Total displacement $u_z$ $\frac{S}{\mu} \rho \left( 1 + \frac{a^2}{\rho^2} \right) \cos \phi$	
$v = \text{Im}(f(z))$	Total displacement $u_z$ $\frac{S}{\mu} \left( \rho \sin \phi + \frac{a^2}{\rho} \sin \phi \right)$			Total displacement $u_z$ $\frac{S}{\mu} \rho \left( 1 - \frac{a^2}{\rho^2} \right) \sin \phi$
Tangent derivative $\frac{\partial u_z}{\partial m}$	$2 \frac{S}{\mu} \cos \phi$	0	$-2 \frac{S}{\mu} \sin \phi$	0
Normal derivative $\frac{\partial u_z}{\partial n}$	0	$2 \frac{S}{\mu} \cos \phi$	0	$2 \frac{S}{\mu} \sin \phi$
Cauchy Riemann equation $\frac{\partial u}{\partial n} = \frac{\partial v}{\partial m}, \frac{\partial u}{\partial m} = -\frac{\partial v}{\partial n}$	Satisfy		Satisfy	

inclusion under the remote anti-plane loading is nothing more than the superposition technique. Following the same example of Lubarda [14] as shown in Fig. 17a, we only considered an inclined elliptic hole under the anti-plane shear loading  $\sigma_{\bar{y}\bar{z}}^\infty$ . By applying the superposition technique for the inclined elliptic hole, the stress and displacement at infinity can be expressed as

$$\sigma_{\bar{y}\bar{z}}^\infty = \sigma_{yz}^\infty \cos \alpha + \sigma_{xz}^\infty \sin \alpha, \text{ and } \bar{u}_{\bar{y}\bar{z}}^\infty = \frac{y}{\mu} \sigma_{yz}^\infty \cos \alpha + \frac{x}{\mu} \sigma_{xz}^\infty \sin \alpha, \tag{88}$$

where  $\alpha$  is the inclined angle of the elliptic hole. The displacement field caused by the remote shear loading is shown below:

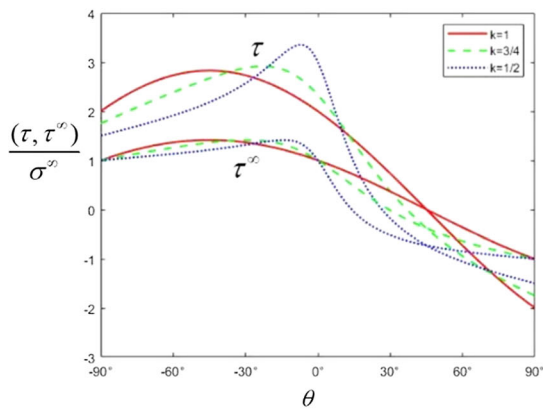
$$\bar{u}_z^\infty(\xi_x, \eta_x) = \frac{S}{\mu} c \sinh \xi_x \sin \eta_x \cos \alpha + \frac{S}{\mu} c \cosh \xi_x \cos \eta_x \sin \alpha. \tag{89}$$

The displacement field caused by infinite plane problem with an elliptic hole is

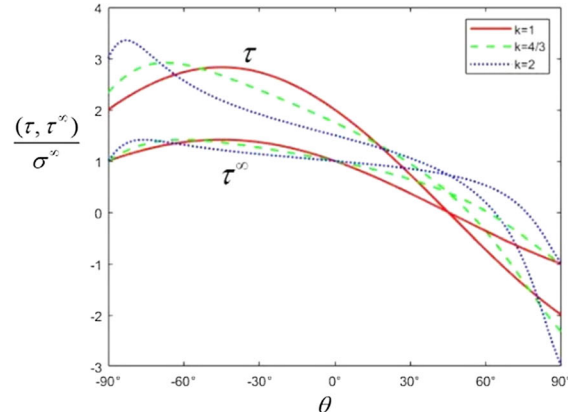
$$\bar{u}_z^M(\xi_x, \eta_x) = \frac{S}{\mu} c e^{\xi_0 - \xi_x} \cosh \xi_0 \sin \eta_x \cos \alpha + \frac{S}{\mu} c e^{\xi_0 - \xi_x} \sinh \xi_0 \cos \eta_x \sin \alpha. \tag{90}$$

**Table 4** The Cauchy–Riemann relation between the elliptic hole and rigid inclusion with respect to different loading

Relation	The reciprocal relation		The reciprocal relation	
Figure				
Function				
B.C.	$t(\nu) = \frac{\partial u_z}{\partial n} = 0, \nu \in B$	$u_z(\nu) = 0, \nu \in B$	$t(\nu) = \frac{\partial u_z}{\partial n} = 0, \nu \in B$	$u_z(\nu) = 0, \nu \in B$
Remote anti-plane shear	$\sigma_{yz}^\infty = S,  y  \rightarrow \infty$	$\sigma_{xz}^\infty = S,  x  \rightarrow \infty$	$\sigma_{xz}^\infty = S,  x  \rightarrow \infty$	$\sigma_{yz}^\infty = S,  y  \rightarrow \infty$
Analytic function $f(z) = u(x, y) + iv(x, y)$ $z = x + iy$	$f(z) = \frac{S}{\mu} \frac{1}{a-b} (a\sqrt{z^2 - c^2} - bz)$		$f(z) = \frac{S}{\mu} \frac{1}{a-b} (az - b\sqrt{z^2 - c^2})$	
$u = \text{Re}(f(z))$	Total displacement $u_z$ $\frac{S}{\mu} c \cos \eta_x (\cosh \xi_x - e^{5i-\xi_x} \cosh \xi_0)$		Total displacement $u_z$ $\frac{S}{\mu} c \cos \eta_x (\cosh \xi_x + e^{5i-\xi_x} \sinh \xi_0)$	
$v = \text{Im}(f(z))$	Total displacement $u_x$ $\frac{S}{\mu} c \sin \eta_x (\sinh \xi_x + e^{5i-\xi_x} \cosh \xi_0)$		Total displacement $u_x$ $\frac{S}{\mu} c \sin \eta_x (\sinh \xi_x - e^{5i-\xi_x} \sinh \xi_0)$	
Tangent derivative $\frac{\partial u_z}{\partial m}$	$\frac{Se^{5i} \cos \eta_x}{\mu \sqrt{\sinh^2 \xi_0 + \sin^2 \eta_x}}$	0	$\frac{-Se^{5i} \sin \eta_x}{\mu \sqrt{\sinh^2 \xi_0 + \sin^2 \eta_x}}$	0
Normal derivative $\frac{\partial u_x}{\partial n}$	0	$\frac{Se^{5i} \cos \eta_x}{\mu \sqrt{\sinh^2 \xi_0 + \sin^2 \eta_x}}$	0	$\frac{Se^{5i} \sin \eta_x}{\mu \sqrt{\sinh^2 \xi_0 + \sin^2 \eta_x}}$
Cauchy Riemann equation $\frac{\partial u}{\partial n} = \frac{\partial v}{\partial m}, \frac{\partial u}{\partial m} = -\frac{\partial v}{\partial n}$	Satisfy		Satisfy	



(a)  $k=1, k=3/4$  and  $k=1/2$



(b)  $k=1, k=4/3$  and  $k=2$

**Fig. 14** The variation of the circumferential stresses  $\tau$  and  $\tau^\infty$  under the remote shear  $\sigma_{yz}^\infty = \sigma_{xz}^\infty = \sigma^\infty$  along the ellipse

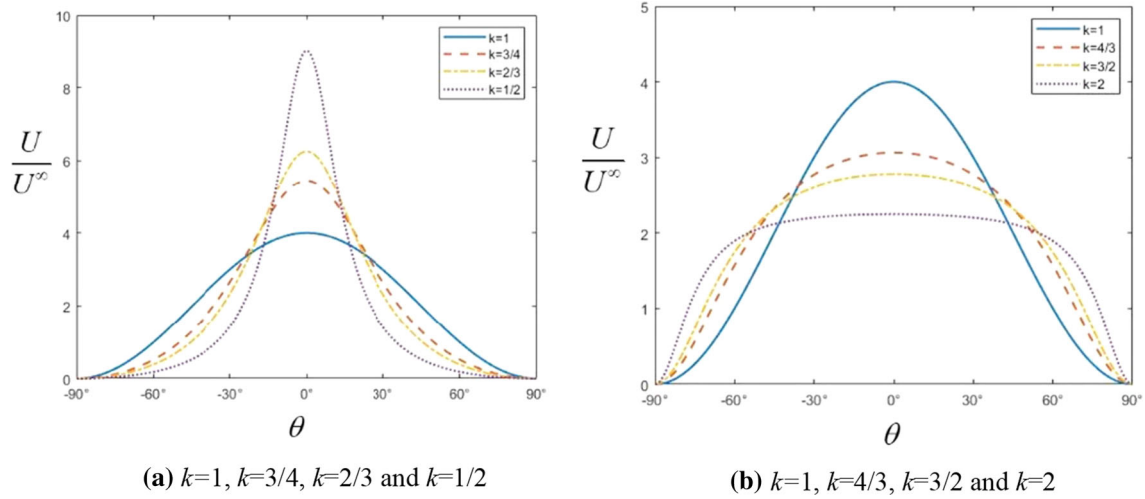


**Fig. 15** The variation of the elastic strain energy density ratio  $U/U^\infty$  under the remote loading  $\sigma_{yz}^\infty \neq 0, \sigma_{xz}^\infty = 0$  along the ellipse

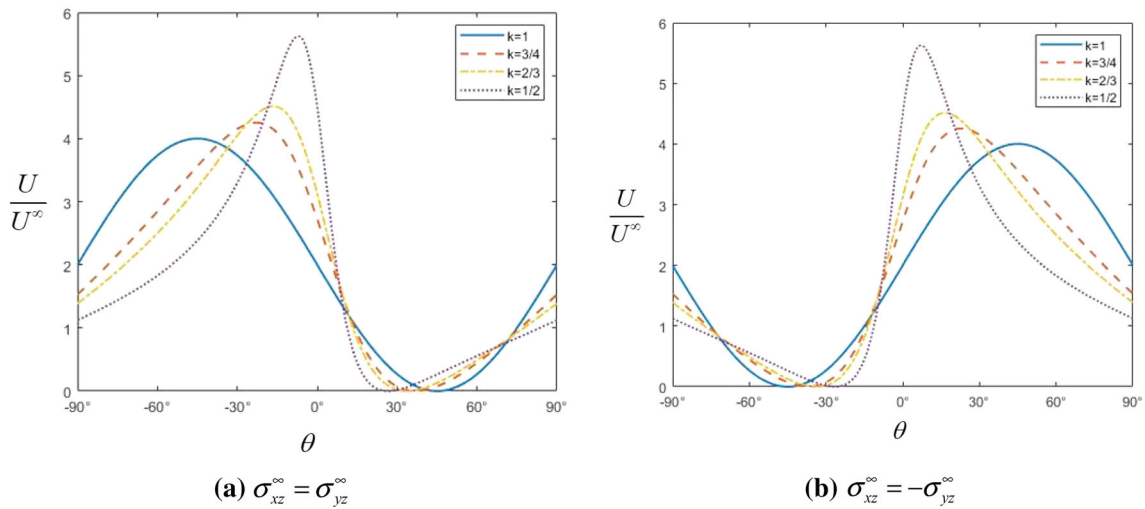


**Fig. 16** The variation of the elastic strain energy density ratio  $U/U^\infty$  under the remote loading for four aspect ratios of  $kx \leq 1$  along the ellipse

Hence, we have the total displacement,

$$\bar{u}_z(\xi_x, \eta_x) = \frac{S}{\mu} c \left( (\sinh \xi_x + e^{\xi_0 - \xi_x} \cosh \xi_0) \sin \eta_x \cos \alpha + (\cosh \xi_x + e^{\xi_0 - \xi_x} \sinh \xi_0) \cos \eta_x \sin \alpha \right). \quad (91)$$

By substituting Eq. (91) into Eqs. (75) and (83), we have

$$\text{SCF} = \left| e^{\xi_0} \cos(\alpha + \eta_x) \sqrt{\frac{2}{(\cosh(2\xi_0) - \cos(2\eta_x))}} \right|, \quad (92)$$

$$\text{SCF} = \left| \frac{e^{\xi_0} \cos(\eta_x + \alpha)}{\sqrt{\sinh^2 \xi_0 + \sin^2 \eta_x}} \right|, \quad (93)$$

respectively. Due to the limited space, we do not report the detailed procedure for the inclined elliptic rigid inclusion case. We only show its final result in Table 5. The inclined elliptic rigid inclusion under the anti-plane shear loading  $\sigma_{yz}^\infty$  is shown in Fig. 17b. The variation of SCF for the inclined elliptic hole with the inclination

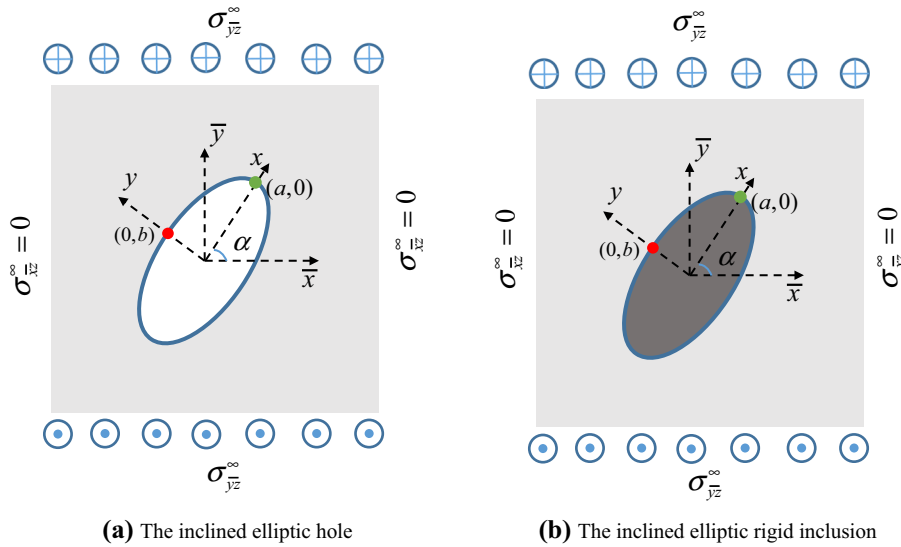


**Fig. 17** The inclined elliptic hole and rigid inclusion in an infinite elastic body under the remote anti-plane loading

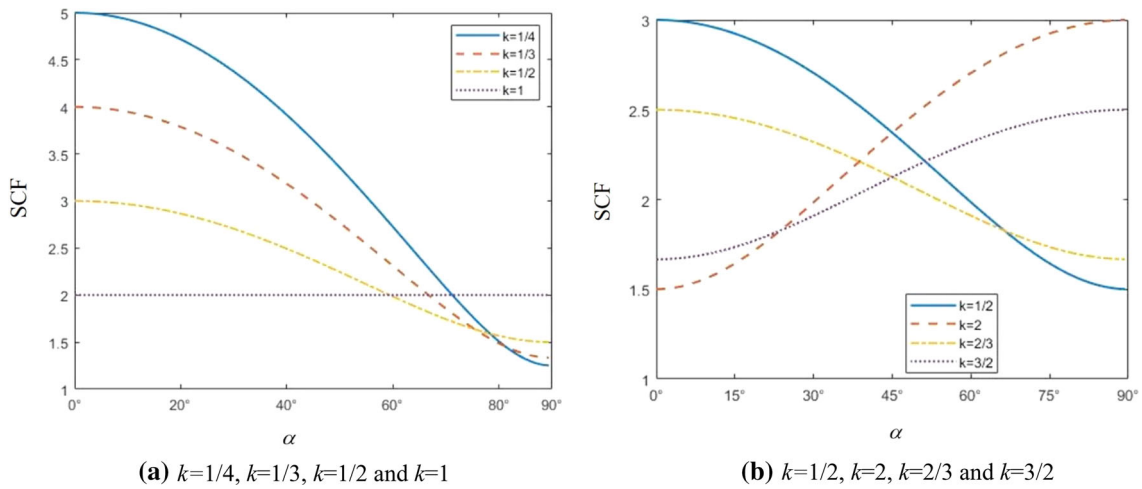


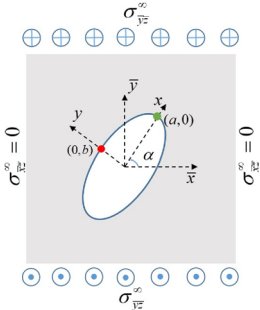
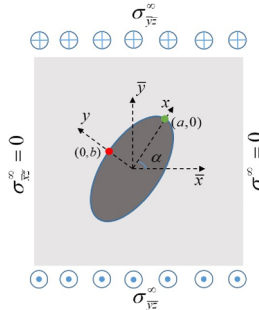
**Fig. 18** The variation of the SCF with the inclination angle  $\alpha$  under the remote loading

angle of  $\alpha$  as well as the various values of  $k$  is plotted in Fig. 18. It should be noted that the SCF of the circular cases can be obtained by using either the polar coordinates or the elliptic coordinates by setting  $k = 1$  to approximate to a circle. All figures match well with those of Lubarda [14] although a different approach using degenerate kernel is employed.

### 6 Conclusions

In this paper, we employed the degenerate kernel in the BIE instead of analytical function in the complex variable to revisit the SCF for the infinite plane containing by a circular/elliptic hole and rigid inclusion under the remote shear. Polar and elliptic coordinates were utilized to represent the degenerate kernel for the circular and elliptic hole and rigid inclusion, respectively. Parameter study of slender ratio of the ellipse as well as the orientation was addressed. Besides, the SCF and the change of elastic strain energy along the boundary due to the hole were investigated to compare with those of Lubarda's paper. All the results and figures for SCF were revisited, and agreement was made. The result show that degenerate kernel can be an alternative tool for solving some BVPs, although complex variable is always employed. Not only the benefits to examine the occurring mechanism of the degenerate scale for the rigid inclusion, but also the reciprocal relation can

**Table 5** The comparison of the results for the inclined elliptic hole and the rigid inclusion

<p>Figure sketch</p>		
<p>Boundary condition</p>	$t(\nu) = \frac{\partial u_z}{\partial n} = 0, \nu \in B$	$u_z(\nu) = 0, \nu \in B$
<p>Stress and displacement at infinity</p>	$\sigma_{yy}^\infty = \sigma_{yy}^\infty \cos \alpha + \sigma_{xz}^\infty \sin \alpha$ $\bar{u}_{yy}^\infty = \frac{y}{\mu} \sigma_{yy}^\infty \cos \alpha + \frac{x}{\mu} \sigma_{xz}^\infty \sin \alpha$	$\sigma_{yy}^\infty = \sigma_{yy}^\infty \cos \alpha + \sigma_{xz}^\infty \sin \alpha$ $\bar{u}_{yy}^\infty = \frac{y}{\mu} \sigma_{yy}^\infty \cos \alpha + \frac{x}{\mu} \sigma_{xz}^\infty \sin \alpha$
<p>Displacement caused by remote shear loading <math>\bar{u}_z^\infty</math></p>	$\frac{S}{\mu} c \sinh \xi_x \sin \eta_x \cos \alpha + \frac{S}{\mu} c \cosh \xi_x \cos \eta_x \sin \alpha$	$\frac{S}{\mu} c \sinh \xi_x \sin \eta_x \cos \alpha + \frac{S}{\mu} c \cosh \xi_x \cos \eta_x \sin \alpha$
<p>Displacement caused by infinite plane problem with an elliptic hole <math>\bar{u}_z^M</math></p>	$\frac{S}{\mu} c e^{-\xi_x} \sin \eta_x \cosh \xi_0 e^{\xi_0} \cos \alpha + \frac{S}{\mu} c e^{-\xi_x} \cos \eta_x \sinh \xi_0 e^{\xi_0} \sin \alpha$	$-\frac{S}{\mu} c e^{\xi_0 - \xi_x} \sinh \xi_0 \sin \eta_x \cos \alpha - \frac{S}{\mu} c e^{\xi_0 - \xi_x} \cosh \xi_0 \cos \eta_x \sin \alpha$
<p>Total displacement <math>\bar{u}_z(\xi_x, \eta_x)</math></p>	$\frac{S}{\mu} c \left( (\sinh \xi_x + e^{-\xi_x} \cosh \xi_0 e^{\xi_0}) \sin \eta_x \cos \alpha \right)$ $+ \frac{S}{\mu} c \left( (\cosh \xi_x + e^{-\xi_x} \sinh \xi_0 e^{\xi_0}) \cos \eta_x \sin \alpha \right)$	$\frac{S}{\mu} c \left( (\sinh \xi_x - e^{\xi_0 - \xi_x} \sinh \xi_0) \sin \eta_x \cos \alpha \right)$ $+ \frac{S}{\mu} c \left( (\cosh \xi_x - e^{-\xi_x} e^{\xi_0} \cosh \xi_0) \cos \eta_x \sin \alpha \right)$
<p><math>\tau</math></p>	$\sqrt{(\sigma_{xz})^2 + (\sigma_{yz})^2} \quad Se^{\xi_0} \cos(\alpha + \eta_x) \sqrt{\frac{2}{\cosh 2\xi_0 - \cos 2\eta_x}}$	$Se^{\xi_0} \sin(\alpha + \eta_x) \sqrt{\frac{2}{\cosh 2\xi_0 - \cos 2\eta_x}}$
	$\tau^m = \frac{\partial u_z}{\partial m} = \frac{\mu}{h} \frac{\partial u_z}{\partial \eta_x} \quad \frac{Se^{\xi_0} \cos(\eta_x + \alpha)}{\sqrt{\sinh^2 \xi_0 + \sin^2 \eta_x}}$	$0$
	$\tau^n = \frac{\partial u_z}{\partial n} = \frac{\mu}{h} \frac{\partial u_z}{\partial \xi_x} \quad 0$	$\frac{Se^{\xi_0} \sin(\eta_x + \alpha)}{\sqrt{\sinh^2 \xi_0 + \sin^2 \eta_x}}$
<p>SCF</p>	$\sqrt{\frac{(\sigma_{xz})^2 + (\sigma_{yz})^2}{\sigma^\infty}} \quad \left  e^{\xi_0} \cos(\alpha + \eta_x) \sqrt{\frac{2}{\cosh 2\xi_0 - \cos 2\eta_x}} \right $	$\left  e^{\xi_0} \sin(\alpha + \eta_x) \sqrt{\frac{2}{\cosh 2\xi_0 - \cos 2\eta_x}} \right $
	$\frac{ \tau^m }{\sigma^\infty} \text{ or } \frac{ \tau^n }{\sigma^\infty} \quad \left  \frac{e^{\xi_0} \cos(\eta_x + \alpha)}{\sqrt{\sinh^2(\xi_0) + \sin^2(\eta_x)}} \right $	$\left  \frac{e^{\xi_0} \sin(\eta_x + \alpha)}{\sqrt{\sinh^2 \xi_0 + \sin^2 \eta_x}} \right $

be understood as the general Cauchy–Riemann formula in terms of the tangent derivative and the normal derivative along the boundary in the present result without using the complex variables. Once the degenerate kernel for the closed-form fundamental solution is available, the BIE is nothing more than the linear algebra and the analytical derivation is possible. Although this application focused on the two-dimensional case, it can be straightforward extended to 3-D problems which cannot be solved by using the complex variables once the corresponding degenerate kernel is available. In addition, the result can be extended to solve a crack problem by setting zero length of minor axis in elliptic coordinates.

**Acknowledgements** Financial support from the Ministry of Science and Technology, Taiwan, under the Grant No. MOST106-2221-E-019-009-MY3 for the National Taiwan Ocean University is gratefully acknowledged.

## References

1. Muskhelishvili, N.I.: Some Basic Problems of the Mathematical Theory of Elasticity. Noordhoff, Leyden (1953)
2. Meguid, S.A., Gong, S.X.: Stress concentration around interacting circular holes: a comparison between theory and experiments. *Eng. Fract. Mech.* **44**, 247–256 (1993). [https://doi.org/10.1016/0013-7944\(93\)90049-X](https://doi.org/10.1016/0013-7944(93)90049-X)
3. Misseroni, D., Corso, F.D., Shahzad, S., Bigoni, D.: Stress concentration near stiff inclusions: validation of rigid inclusion model and boundary layers by means of photoelasticity. *Eng. Fract. Mech.* **121–122**, 87–97 (2014). <https://doi.org/10.1016/j.engfracmech.2014.03.004>
4. Setiawan, Y., Gan, B.S., Han, A.L.: Modeling of the ITZ zone in concrete: experiment and numerical simulation. *Comput. Concr.* **19**, 647–655 (2017). [10.12989/cac.2017.19.6.647](https://doi.org/10.12989/cac.2017.19.6.647)
5. Chen, Y.Z., Lin, X.Y., Wang, Z.X.: Evaluation of the degenerate scale for BIE in plane elasticity and antiplane elasticity by using conformal mapping. *Eng. Anal. Bound. Elem.* **33**(2), 147–158 (2009). <https://doi.org/10.1016/jenganabound.2008.05.007>
6. Zou, W.N., Lee, Y.G., He, Q.C.: Inclusions inside a bounded elastic body undergoing anti-plane shear. *Math. Mech. Solids* **23**(4), 1–18 (2017). <https://doi.org/10.1177/1081286516681195>
7. Ru, C.Q., Schiavone, P.: A circular inhomogeneity with circumferentially inhomogeneous interface in anti-plane shear. *Proc. R. Soc. A* **453**, 2551–2572 (1997). <https://doi.org/10.1098/rspa.1997.0136>
8. Savruk, M.P., Kazberuk, A., Tarasyuk, G.: Stress concentration near holes in the elastic plane subjected to antiplane deformation. *Mater. Sci.* **48**(4), 415–426 (2009). <https://doi.org/10.1007/s11003-013-9521-6>
9. Kohno, Y., Ishikawa, H.: Singularities and stress intensities at the corner point of a polygonal hole and rigid polygonal inclusion under antiplane shear. *Int. J. Eng. Sci.* **33**, 547–560 (1995). [https://doi.org/10.1016/0020-7225\(95\)00023-Q](https://doi.org/10.1016/0020-7225(95)00023-Q)
10. Corso, F.D., Shahzad, S., Bigoni, D.: Isotoxal star-shaped polygonal voids and rigid inclusions in nonuniform antiplane shear fields. Part I: formulation and full-field solution. *Int. J. Solids Struct.* **85–86**, 67–75 (2016). <https://doi.org/10.1016/j.ijsolstr.2016.01.027>
11. Corso, F.D., Shahzad, S., Bigoni, D.: Isotoxal star-shaped polygonal voids and rigid inclusions in nonuniform antiplane shear fields. Part II: singularities, annihilation and invisibility. *Int. J. Solids Struct.* **85–86**, 76–88 (2016). <https://doi.org/10.1016/j.ijsolstr.2016.01.026>
12. Shahzad, S., Niiränen, J.: Analytical solution with validity analysis for an elliptical void and a rigid inclusion under uniform or nonuniform anti-plane loading. *Theor. Appl. Fract. Mech.* **97**, 62–72 (2018). <https://doi.org/10.1016/j.tafmec.2018.07.009>
13. Savin, G.M.: Stress Concentration Around Holes. Pergamon Press, New York (1961)
14. Lubarda, V.A.: On the circumferential shear stress around circular and elliptical holes. *Arch. Appl. Mech.* **85**(2), 223–235 (2015). <https://doi.org/10.1007/s00419-014-0915-1>
15. Noda, N.A., Takase, Y.: Stress concentration formula useful for all notch shape in a round bar (comparison between torsion, tension and bending). *Int. J. Fatigue* **28**, 151–163 (2006). <https://doi.org/10.1016/j.ijfatigue.2005.04.015>
16. Honein, E., Honein, T., Herrmann, G.: On two circular inclusions in harmonic problems. *Q. Appl. Math.* **50**, 479–499 (1992). <https://doi.org/10.1090/qam/1178429>
17. Chen, J.T., Wu, A.C.: Null-field approach for the multi-inclusion problem under antiplane shears. *ASME J. Appl. Mech.* **74**(3), 469–487 (2006). <https://doi.org/10.1115/1.2338056>
18. Golberg, M.A.: Solution Methods for Integral Equation. Plenum Press, New York (1978)
19. Galybin, A.N.: Formation of cracks on compressing an unbounded brittle body with a circular opening. *J. Appl. Math. Mech.* **49**, 797–799 (1985). [https://doi.org/10.1016/0021-8928\(85\)90021-8](https://doi.org/10.1016/0021-8928(85)90021-8)
20. Cochran, J.A.: Applied Mathematics: Principles, Techniques, and Applications. Wadsworth Pub Co, Belmont (1982)
21. Lee, Y.T., Chen, J.T.: Null-field approach for the antiplane problem with elliptical holes and/or inclusions. *Compos. B Eng.* **44**, 283–294 (2013). <https://doi.org/10.1016/j.compositesb.2012.05.025>
22. Noda, N.A., Hayashida, H.: Interaction between elliptical and ellipsoidal inclusions under bending stress fields. *Arch. Appl. Mech.* **70**, 612–624 (2000). <https://doi.org/10.1007/s004190000093>
23. Milne-Thomson, L.M.: Theoretical Hydrodynamics, 5th edn. Macmillan & Co Ltd, New York (1968)
24. Chen, J.T., Chiu, Y.P.: On the pseudo-differential operators in the dual boundary integral equations using degenerate kernels and circulants. *Eng. Anal. Bound. Elem.* **26**, 35–41 (2002). [https://doi.org/10.1016/S0955-7997\(01\)00087-X](https://doi.org/10.1016/S0955-7997(01)00087-X)
25. Morse, P.M., Feshbach, H.: Methods of Theoretical Physics. McGraw-Hill, New York (1978)
26. Lubarda, V.A.: Circular inclusions in anti-plane strain couple stress elasticity. *Int. J. Solids Struct.* **40**(15), 3827–3851 (2003). [https://doi.org/10.1016/S0020-7683\(03\)00227-0](https://doi.org/10.1016/S0020-7683(03)00227-0)

**Publisher's Note** Springer Nature remains neutral with regard to jurisdictional claims in published maps and institutional affiliations.